九州大学学術情報リポジトリ
Kyushu University Institutional Repository

Microstructural Analysis of IGZO Thin Films and Its Thin-Film Transistor Application

エムデイ, ローフ, ウル, カリム, カン

https://hdl.handle.net/2324/4784650

出版情報：Kyushu University, 2021, 博士（学術）, 課程博士
バージョン：
権利関係：

Microstructural Analysis of IGZO Thin Films and Its Thin-Film Transistor Application

Dissertation

Doctor of Philosophy

By

MD RAUF UL KARIM KHAN

B. Sc. (AIUB, Bangladesh), M. Eng. (KU, Japan)

Department of Applied Science for Electronics and Materials

Interdisciplinary Graduate School of Engineering Sciences

Kyushu University

Japan

October 2021

Dedicated to

My Parents

&

Family

Abstract

Indium-Gallium-Zinc Oxide (IGZO) thin films have received great attention in Display technology because of their good electrical, electronic and optical properties. Their electronic device applications are being enhanced owing to their remarkable performance, e.g., high electron carrier mobility, better uniformity over a large area, and potential optical transparency. Moreover, IGZO can be a promising thermoelectric candidate for its good thermoelectric performance to other oxide candidates. The thermal conductivity of IGZO indicates its ability for heat conduction, which is subjected to various factors, and can be subdivided into electro- and phono-thermal conductivities revealed by phonon–phonon and electron–electron scattering. Most studies on IGZO thin films focused on electrical, electronic, and optical properties . The thermal properties of IGZO thin films are also of vital importance for heat dissipation and thermal management of devices. Although the atomic-scale structure of IGZO films has been lacked to reveal whether these are amorphous or crystalline, few fundamental studies have been performed on the relationship between the thermal conductivity and microstructure of IGZO thin films.

From the above perspective, this thesis emphases towards the development of the relationship between the temperature dependence of thermal conductivity of the Indium–Gallium–Zinc–Oxide (IGZO) thin films and microstructure analysis. The research strongly stress on two factors, firstly, Scanning transmission electron microscopy (STEM) observations were also carried out to characterize the nanometre-scale microstructure of the IGZO thin film. Secondly, the temperature dependence thermal conductivity of the Indium–Gallium–Zinc–Oxide (IGZO) thin films was investigated with the differential three-omega method (3ω) for the clear demonstration of nano-crystallinity. Electron microscopy

observations revealed the presence of nanocrystals embedded in the amorphous matrix of the IGZO films. The typical size of the nanocrystals was approximately 2 to 5 nm with the lattice distance of about 0.24 nm to 0.26 nm. These experimental results indicate that the nanocrystalline micro-structure controls the heat conduction in the IGZO films. To perform the differential three-omega (3ω) method experiment, the IGZO thin films were deposited on an alumina (α-Al_2O_3) substrate by direct current (DC) magnetron sputtering at different oxygen partial pressures ([PO_2] = 0 %, 10 %, and 65 %). Their thermal conductivities at room temperature were measured to be 1.65, 1.76, and 2.58 $Wm^{-1}K^{-1}$, respectively. The thermal conductivities decreased with increase in the ambient measurement temperature. This thermal property is similar to that of crystalline materials.

To analyse the IGZO thin-film transistor application, the back-channel etched Indium–Gallium–Zinc–Oxide (IGZO) thin-film transistors (TFTs) with copper (Cu) source and drain (S/D) which are patterned by a selective etchant was fabricated and investigated the electrical properties. The main challenge of this work strongly stress on two factors, firstly patterned the source and drain contact by photolithography process with special Cu etchant without damaging the IGZO layer. Secondly, to protect the Cu diffusion into the IGZO thin film. The fabrication process parameters are optimized and the electrical properties is discussed. The Cu S/D were fabricated on molybdenum (Mo) layer to prevent the Cu diffusion to the active layer (IGZO). In this work, the IGZO TFTs with Mo/Cu S/D exhibits good electrical properties as the linear region mobility is 12.3 cm^2/V-s, saturation region mobility is 11 cm^2/V-s, threshold voltage is 1.2 V and I_{ON} is 3.16 x 10^{-6} A. The results suggested an effective fabrication method for fabricating high mobility metal oxide TFT based on Cu S/D.

Acknowledgements

First of all I show my heartiest gratitude to the almighty ***Allah*** who has given me the strength and ability to do the research and writing the thesis.

Then, I would like to express my deepest sense of gratitude and indebtedness to my supervisor, ***Professor Reiji HATTORI***, for giving me the opportunity to perform this significant research in his laboratory under his supervision. In particular, all the suggestions and recommendations of my supervisor during my research have been invaluable and appreciated.

I am indebted to ***Dr. Shim-Chang Hoon***, for his valuable guidance and providing me the opportunity to discuss technical results of this work any time.

I acknowledge my thanks to ***Dr. Agung Imaduddin*** for hosting the domestic internship in Indonesian Institute of Sciences, Indonesia. I am very grateful to ***Professor Jin-Seong Park,*** to give me the opportunity to work with him in Hanyang University, Korea.

I would like to express my gratefulness to ***Professor Michitaka OHTAKI and Professor Satoshi HATA*** for evaluating this work, and their valuable assistance, guidelines and comments.

I am thankful to ***Professor Koji MIYAZAKI*** and ***Associate Professor Tomohide YABUKI, Kyushu Institute of Technology, Kitakyushu, Japan*** for providing me a great

chance to discuss and do some experiment in his laboratory. His wise guidance and support helped me a lot during my doctoral study.

I am thankful to all of my present and former laboratory members and staff for their help and kind cooperation.

I express my humble obligation to my affectionate and loving father, mother, sisters, brother, In-laws for their love, inspiration and prayers for me. In particular, I am thankful and would like to express my gratitude to my father ***Md. Rezaul Karim Khan*** and mother ***Shefali Begum***, sisters ***Rezwana Karim Khan & Raihana Karim Khan***, and brother ***Rakibul Karim Khan*** for everything they have done for me.

I wish to express my heartfelt indebtedness ***Advanced Graduate Program in Global Strategy for Green Asia (GA), IGSES, Kyushu University*** for providing scholarship and all other facilities required in this study.

Finally, I wish to thank my beloved wife ***Farhana Nur Rahman*** for understanding me, always having patience, encouraging me during my study and giving me the best gift of my life, my daughter, ***Farheen Khan***.

MD. RAUF UL KARIM KHAN

Kyushu University, Japan

Contents

Abstract i

Acknowledgements iii

List of Figures vii

List of Tables 10

Chapter 1 Introduction 11

1.1 Background 11

1.2 Motivation 14

1.3 Objectives of the Research 15

1.4 Organization of the thesis 15

Chapter 2 Microstructure Analysis of IGZO Thin Film 18

2.1 Introduction 18

2.2 Scanning Transmission Electron Microscopy 20

2.2.1 Overview 20

2.2.2 STEM detectors and imaging mode 22

2.3 Sample Preparation 23

2.3.2 Microstructure Analysis 29

2.4 Conclusion 35

Chapter 3 Overview of the Thermal Conductivity Characterization Techniques for Thin Films 36

3.1 Electrical heating and sensing techniques 38

3.2 Cross-plane thermal conductivity measurement of thin-film 39

3.2.1 The Three – Omega (3ω) Method 39

3.2.2 Steady – State Method 42

3.3 In-plane thermal conductivity measurement of thin-film 42

3.3.1 Membrane Method 43

3.3.2 Bridge Method 47

3.3.3 Heat spreading Method 47

Chapter 4 Temperature Dependence Thermal Conductivity of IGZO Thin Films 48

4.1 Temperature Dependence Thermal Conductivity Measurement Using 3ω Method 50
4.2 Estimation of Mean-Free Path 55
4.3 Conclusions 57

Chapter 5 Application of Indium Gallium Zinc Oxide (IGZO) Thin Film Transistor Application........58

5.1 Overview of Indium Gallium Zinc Oxide TFTs 58
5.1.1 Amorphous Hydrogenated Silicon (a-Si:H) TFTs 59
5.2 Amorphous Oxide TFTs 61
5.3 Current issues on TFT technology 62
5.4 Experiments 63
5.4.1 Fabrication process 63
5.5 Conclusion 73

Chapter 6 Conclusions and Recommendations........74

6.1 Introduction 74
6.1.1 Microstructure analysis of IGZO thin films 74
6.2 Application to IGZO TFTs: 75
6.3 Future Recommendation 76

References........77

List of Figures

Figure 1.1: Important applications of IGZO TFTs. [5] 11

Figure 1.2: Historical improvement of oxide semiconductor based TFT devices [13]. 12

Figure 2.1: Schematic of STEM mode. 22

Figure 2.2: The principle of Focus Ion Beam milling. 23

Figure 2.3: FIB milling Process 24

Figure 2.4: Sample Preparation using FIB milling (a)1st milling step, (b) 2nd milling step, (c) transfer the sample from specimen substrate using needle, (d) fixed on the sample holder (e) 3rd milling step, (f) 4th milling step (g) Bright-field (BF) transmission electron microscopy (TEM) image of a cross-sectional IGZO/α-Al_2O_3 film indicating Ga ion beam damage (red box), (g) a cross-sectional BF-TEM image after subsequent low-power Ar milling that effectively removed the damaged layer on the cross-sectional specimen (red box), and (h) a plan-view secondary-ion microscopy image of the thin foil specimen with a thickness less than 50 nm prepared by the Ga/Ar ion beam-milled Sample B. 29

Figure 2.5: Cross-sectional scanning transmission electron microscopy (STEM) observation of Sample B. (a) and (b)Annular dark-Field (ADF) STEM image in different position. 32

Figure 2.6: (a) and (b) selective area diffraction pattern acquired from the IGZO film under the TEM (parallel beam) mode at different region of specimen. 34

Figure 2.7 (a) and (b) lattice distance in two different regions 35

Figure 3.1: Sample configuration and challenges of the characterization [22]. 37

Figure 3.2: Cross-plane thermal conductivity characterization strategy. 39

Figure 3.3: (a) Schematic diagram of sample and reference, (b) example of the experimental method [22]. 42

Figure 3.4: In-plane thermal conductivity measurement strategies 43

Figure 3.5: Important experimental methods for in-plane thermal conductivity characterization: (a) membrane method, (b) bridge method, and (c) in-plane heat spreading method using buried thermal barriers with narrow width wire [22]. 46

Figure 4.1: Plan view of the shadow mask of the heater with the length of 15 mm, width of 10 mm and a thickness of 20 µm (a) and the schematic diagram of a film sample (b) and the reference (c). 50

Figure 4.2: Temperature oscillation Amplitude of (a) Sample A, (b) Sample B, and (c) Sample C at room temperature. 53

Figure 4.3: Temperature dependence of thermal conductivity of IGZO thin films in the temperature range from room temperature to 373 K. 54

Figure 4.4: Young's modulus with various indentation depths of 500 nm IGZO thin films 56

Figure 5.1: Requirement of mobility for higher-definition FPDs 62

Figure 5.2: Diagram of the DC magnetron sputtering process [74] 64

Figure 5.3: Process flow of bottom gate top contact IGZO TFTs. 65

Figure 5.4: Microscopic image of bottom gate top contact IGZO TFTs after using the special Cu etchant 66

Figure 5.5: Schematic cross-section of IGZO TFT on a glass substrate with bottom gate top contact structure. (a) sample A, (b) Sample B, and (c) top view of IGZO TFTs. 67

Figure 5.6: (a) Output and (b) transfer characteristics of sample A without annealing after deposition Cu S/D electrode. 69

Figure 5.7: (a) Output and (b) transfer characteristics of sample A with annealing after deposition of CU S/D electrode. 71

Figure 5.8: (a) Output and (b) transfer characteristics of sample B after annealing with Mo/Cu S/D electrodes. 72

List of Tables

Table 1.1 Summary of the comparison of the Different TFT technologies for next generation display technology. 13

Table 5.1: Comparison of different TFT technologies 60

Table 5.2: Electrical performance of sample A and B after post annealing 73

Chapter 1

Introduction

1.1 Background

Metal oxide semiconductor especially indium gallium zinc oxide (IGZO) based thin films, have attracted huge research attention in display technology because of high electron carrier mobility, better uniformity over sizeable area and good optical transparency [1–3]. Nomura et al. reported first the amorphous and single crystalline IGZO active layer based thin film transistors (TFTs) in 2004 [4]. Figure 1.1 shows some important application based on IGZO TFTS.

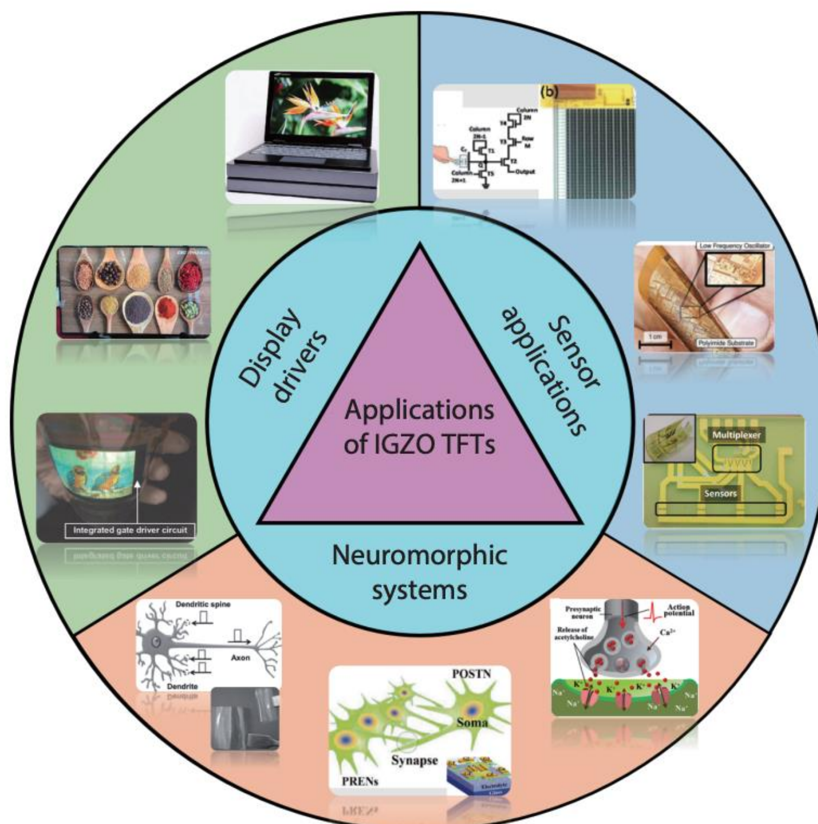

Figure 1.1: Important applications of IGZO TFTs. [5]

Compared with low-temperature poly-silicon (LTPS) and hydrogenated amorphous silicon (a-Si:H) TFTs, the IGZO TFT technologies are rapidly gaining popularity for enabling flexible or stretchable displays [6] [7]. Moreover, ZnO active-channel TFTs are promising solutions to high-resolution display technologies but are not suitable for large-area display applications owing to their small feature sizes[8]. Hsieh et al. fabricated ZnO TFTs with varying active-channel lengths and widths and achieved a saturation region mobility of >8 cm^2/Vs [9]. Concurrently, Yabuta et al. employed amorphous IGZO (a-IGZO) active channels in TFTs and observed good electrical properties, which indicate the possibility of large-area, high-resolution, and integrated circuit (IC) applications [1]. In transparent IGZO TFTs, it was first used as a single crystalline active channel material because of its high electron mobility (80 $cm^2/(Vs)$) [10]. On the other hand, a-IGZO is also popular for stretchable or flexible electronics for its capability to be fabricated at room temperature with high mobility (μ >10 $cm^2/(Vs)$) [11]. Figure 1.2 shows the historical overview of the development of oxide semiconductor based TFT devices. Moreover, IGZO can be a promising thermoelectric candidate for its comparable thermoelectric performance to other oxide candidates [12].

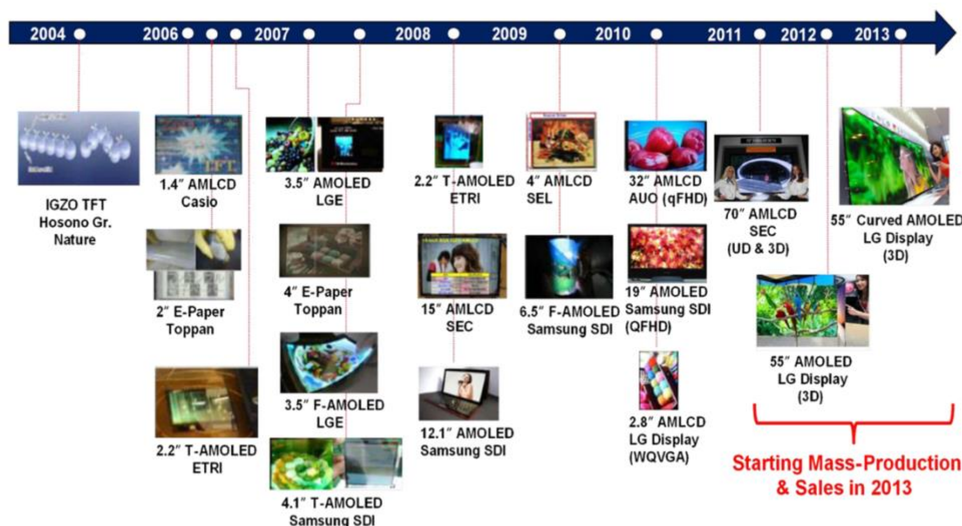

Figure 1.2: Historical improvement of oxide semiconductor based TFT devices [13].

Recently, IGZO TFTs are used as a switching device in the flat panel display such as active-matrix organic light-emitting diode (AMOLED) displays, active-matrix liquid crystal displays (AMOLCD) and electrophoretic displays [14][15]. Table 1.1 Summary of the comparison of the Different TFT technologies for next generation display technology. It is clear that a prospective semiconductor material is highly desired with high mobility and uniformity over large area capability. As increasing the resolution (≥ 8 K), display size (≥ 110 inch) and high frame rate (≥ 480 Hz) for the flat panel display; the low-resistance metals are remarkably required for the source (S) and drain (D) electrodes. Because it will help to reduce resistance-capacitance (RC) delay of display panel to avoid image distortion and shading [16].

Table 1.1 Summary of the comparison of the Different TFT technologies for next generation display technology.

Materials of Active Layer	Mobility (cm^2/Vs)	Visible Light Transparency	Uniformity Over large Area	Features
a-Si:H	< 1	Poor	Good	Low mobility
Poly-Si	~ 100	Poor	Poor	Required addition process for crystallization
ZnO	20 ~ 50	Good	Poor	High tendency to form poly phase
IGZO	3 ~ 12	Good	Good	Balanced

				between uniformity and mobility

1.2 Motivation

The motivation of this research is originated from the lack of detail studies on microstructure analysis of IGZO thin films and Cu S/D IGZO TFTs. IGZO can be a promising thermoelectric candidate for its good thermoelectric performance to other oxide candidates. The thermal conductivity of IGZO indicates its ability for heat conduction, which is subjected to various factors, and can be subdivided into electro- and phono-thermal conductivities revealed by phonon–phonon and electron–electron scattering. The thermal properties of IGZO thin films are also of vital importance for heat dissipation and thermal management of devices. Fundamental studies are needed to reveal the relationship between the thermal conductivity and microstructure of IGZO thin films. There is an argument about the microstructure of IGZO thin films. So the atomic-scale structure of IGZO films is important to investigate whether these are amorphous or crystalline.

In the TFT application, the low-resistance metals such as Cu has attracted more attention as a S/D electrodes to reduce resistance-capacitance (RC) delay but there is a big challenge to pattern the Cu S/D selectively using photolithography process without damaging the active layer (IGZO). Most of the Cu etchant are acidic which can damage the IGZO layer easily. Another concern is to prevent the Cu diffusion into the IGZO layer. The diffusion of Cu into IGZO deteriorates the electrical performance because it is acting as acceptor-like trap states of IGZO TFT.

1.3 Objectives of the Research

To achieve the above-mentioned problem statement, following initiatives have been taken and the results are reported in this thesis:

I. Scanning transmission electron microscopy (STEM) observations has carried out to confirm the presence of nanocrystals embedded in the amorphous matrix of the IGZO films.

II. The temperature dependence of thermal conductivity of the Indium–Gallium–Zinc–Oxide (IGZO) thin films has investigated with the differential three-omega method for the clear demonstration of nano-crystallinity.

III. The electrical performance of the back-channel etched Indium–Gallium–Zinc–Oxide (IGZO) thin-film transistors (TFTs) with copper (Cu) source and drain (S/D) has investigated. The Cu S/D was fabricated on molybdenum (Mo) layer to prevent the Cu diffusion in the active layer (IGZO).We deposited the Cu layer using thermal evaporation and performed the selective wet etching of Cu using non-acidic special etchant without damaging the IGZO active layer.

1.4 Organization of the thesis

The thesis includes six chapters explaining the various theoretical and experimental findings. Microstructure analysis, temperature dependence of Thermal conductivity utilizing Three-omega method and back-channel etched IGZO TFTs have been studied. The arrangement of the thesis is as follows:

Chapter 1: Introduction

Chapter 2: Microstructure Analysis of IGZO Thin Film

Chapter 3: Overview of the Thermal Conductivity Characterization Techniques for Thin Films

Chapter 4: Temperature Dependence of Thermal Conductivity of IGZO Thin Films

Chapter 5: Application to Indium Gallium Zinc Oxide (IGZO) Thin Film Transistor Application

Chapter 6: Overall conclusion and future recommendation

The key points of each chapter are given:

CHAPTER 1

The chapter covers on the introduction to the IGZO thin films and TFTs, a summary of the different TFT technologies, motivation, aim of this research. Finally, this chapter clarifies the motivation and objectives of the thesis.

CHAPTER 2

The chapter illustrates the brief introduction of microscope features of scanning transmission electron microscope. It also presents the specimen preparation for scanning transmission electron microscopy(STEM) analysis using focus ion beam (FIB) milling process. Detail explanation of microscopic image is covered to understand whether the IGZO thin film is amorphous or crystalline. Further analysis of the annular dark-field STEM observation and selective area diffraction patterns are analysed to calculate the crystal size and lattice distance.

CHAPTER 3

The chapter covers the overview of the thermal conductivity characterization techniques for thin films to make the comparison. The theory and measurement process of the Three-Omega (3ω) method is described in this chapter. The advantages and disadvantages and the solution to the characterization methods are also included.

CHAPTER 4

The chapter explains the brief sample preparation process for the temperature dependence of thermal conductivity using the 3ω method. This chapter also includes the temperature dependence thermal conductivity characterization of the Indium–Gallium–Zinc–Oxide (IGZO) thin films utilizing the differential three-omega (3ω) method. Instead of results analysis, the phonon mean free path is estimated. Finally, this chapter includes the circumstantial conclusion of this research and clarifies the relationship between the temperature dependence thermal conductivity of IGZO thin films and microstructure.

CHAPTER 5

The chapter is covers the brief introduction and electrical characteristics analysis of IGZO TFTs, which clearly clarify the effect of Cu diffusion into IGZO thin film. Next, the work covers the electrical properties analysis and uses of the selective Cu etch which can etch the without damaging the IGZO layer.

CHAPTER 6

The chapter concludes the thesis ends with the major findings where the originality and contribution of the author, and recommendations for future improvement, have been made.

Chapter 2

Microstructure Analysis of IGZO Thin Film

2.1 Introduction

The preliminary aim of microscopy is to uncover objects those are very tiny not to be seen by eyes. The human eyes can not discover the objects which are too small as a few tens micrometer. There are many objects and structures that affect and control our daily life, which order of magnitude is smaller not able to observe by eyes. Microscopes are an important tool to explore and understand objects such as grain structure of crystalline materials, nano crystallinity, individual cells and viruses. Microscope surpass the natural physical limits and help to understand details of the environment. So, microscopes are the key to unlock the micro and nano universe. Every microscopy has specific characteristics to characterise the object. Indeed, it is completely unusual to unravel the whole nature of the object, most cases known part is analyzed quite a lot. Typically, there is an available priori information in the database, and there are specific questions which are needed to address during microscopic observation. The microscope reveals the form of magnified image of an object and unknots the unknown questions. The magnified image is supposed to reflect certain characteristics of a given object, such as its constitution, structure and shape. The microscope produces the details of the image which is not possible to see by eye. Although the image is never equivalent to the object. An image is all about an interpretation of the

object. In the microscopy, the interpretation is strongly associated with the proof or the radiation which is used to explore the object.

By utilizing conventional optical microscope, the observation can be expand down to the objects that are bit smaller than a micrometer. Even though the image form is substantially better than what is doable with a normal vision of eyes. Although it is still very insufficient to resolve the atomic structure analysis of the materials. So the basic skeleton of materials is remaining out of reach. In order to understand the fundamental constitution of materials such as structure and physical properties, it is necessary to measure the information about materials' atomic framework. As a diffraction techniques, Neutron and X-ray diffraction are powerful to capture atomic structure information but diffraction pattern does not contain any local information. To analyze the species of atom, location of individual atom, measuring element of atom and how it is connected with the neighboring atom; structural and local information is very important.

Electron microscopy offers the opportunity to observe the materials which have smaller accessibility by optical microscope. Instead of optical light, transmission electron microscopy and scanning electron microscopy employ electron with energies between 50 to 1000 keV. The wavelength of electrons in between 5 and 1 pm. So that the magnitude of resolving conventional high resolution microscope is two order larger. This resolution is enough sufficient to access some kind of atomic resolution information, though the atom spacing on crystal lattice is in the order's range of 200 pm. Electron microscopy is enough good for atomic resolution imaging at but it is not effective for those materials whose surface atom can remove quite easily. The electron can damage the materials significantly. Furthermore, the resolution problem of conventional electron microscopy is not only related to the electron wavelength. There are many other factors which can affect the resolution of the microscope. One factor is aberration effect, i.e. non ideal imaging characteristics of lenses. The aberration

effect of image characterization carry the false or truncsted object informstion. The image is comprises a wrong interpretation of an object. The light and electron optics are not equivalent regarding aberrations. For this reason, the imaging characteristics of electron lenses are not perfect. Surely, there is no real light optical lenes which are perfect. Serial arrangement of convex and concave lenses can compensate for the aberration effect.

The resolution limitation imposed by the aberrations but it does not mean that there is no object information in resolution limit micrograph. Modern but conventional electron microscopes transfer the object information to the image, which reaches beyond the actual resolution limit. However, the high resolution is not free from aberration effect. Though we can not read it from the micrograph directly. Hence, atomic resolution imaging is workable with scanning electron microscopes, as lens aberration may cause image artifacts. The image artifacts obscure the object information in a micrograph. By correcting the intrinsic aberrations of round electromagnetic electron lenses, the aberration effect can be minimized. Aberration-corrected image is the formation of micrographs which no longer suffer from aberrations. Thus, it shows an improved resolution which contains accurate information and simple interpretation of the object.

This chapter covers the Scanning transmission electron microscopy (STEM) observations we to characterize the nanometer-scale microstructure of the IGZO thin film. The specimen preparation process is also described elaborately.

2.2 Scanning Transmission Electron Microscopy

2.2.1 Overview

A scanning transmission electron microscope (STEM) is a type of transmission electron microscope (TEM). By passing through a sufficiently thin specimen, the conventional transmission electron microscopy image is formed. In STEM, the electron beam is focused on

a fine spot and scanned all over the sample in a raster illumination system constructed. For this reason, the sample is illuminated at each point with the beam parallel to the optical axis. Typically the spot size is 0.05 - 0.2 mm. The rastering of the beam across the sample makes suitable analytical techniques such as Z-contrast annular dark-field imaging, and spectroscopic mapping by energy dispersive X-ray (EDX) spectroscopy, or electron energy loss spectroscopy (EELS). Figure 2.1 shows the schematic of scanning transmission electron microscopy mode.

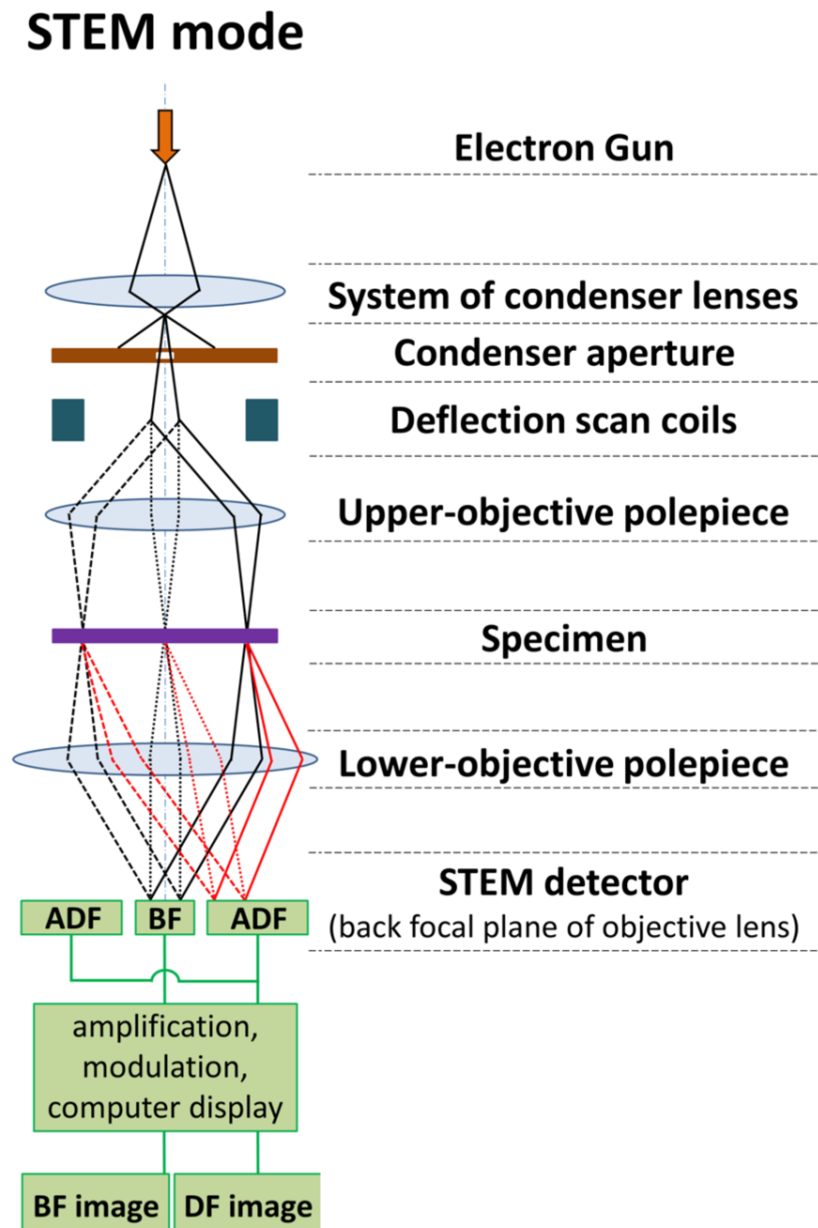

Figure 2.1: Schematic of STEM mode.

2.2.2 STEM detectors and imaging mode

2.2.2.1 Annular Dark – Field Imaging

Annular dark-field imaging is a method of mapping of samples in a STEM. These images are formed by collecting the scattered electrons by using annular dark-field detector. In conventional TEM, an objective aperture is used to form dark-field imaging, which only collects scattered electrons that pass through. In contrast, STEM dark-field imaging uses an annular detector to collect only scattered electrons, but not use any aperture to differentiate the scattered electrons from the main beam. Consequently, the contrast mechanisms are different between conventional dark field imaging and annular dark field. An annular detector collects electrons from an annulus around the beam and it can sampling more scattered electrons than can pass through an objective aperture. This allows the main beam to pass to an electron energy loss spectroscopy (EELS) detector. Annular dark field imaging is commonly performed in parallel to bright-field STEM imaging and in parallel with energy-dispersive X-ray spectroscopy.

2.2.2.2 Bright-Field Imaging

Bright-field detector of STEM is located in the path of the transmitted electron beam. The Axial bright-field detectors are located in the centre of the illumination of the transmitted beam. This detector collects the electrons transmitted in the path of the beam close to the optical axis. It often provides complementary images of annular dark-field imaging. Sometimes, the bright-field detectors have been used to obtain atomic resolution image.

2.3 Sample Preparation

2.3.1.1 Thin Film Deposition

A 500 nm IGZO (In:Ga:Zn = 1:1:1) thin films with were deposited on an alumina substrate by DC magnetron sputtering method at room temperature. The deposition rate of IGZO is around 2.5 nm/min. A mixture of Ar and O_2 gas was used during the sputtering process. The oxygen partial pressure [PO_2] was calculated from the ratio of O_2 gas flow rate and total Ar/O_2 flow rates. Three samples at various [PO_2] such as [PO_2] = 0 % (Sample A), [PO_2] = 10 % (Sample B, and [PO_2] = 65 % (Sample C) were deposited for pursuing the measurement.

2.3.1.2 Sample preparation using FIB milling for STEM Analysis

The focus ion beam (FIB) milling technique is commonly use to prepare the sample for transmission electron microscope or scanning transmission electron microscope analysis. The sample should be very thin around 100 nm or less.

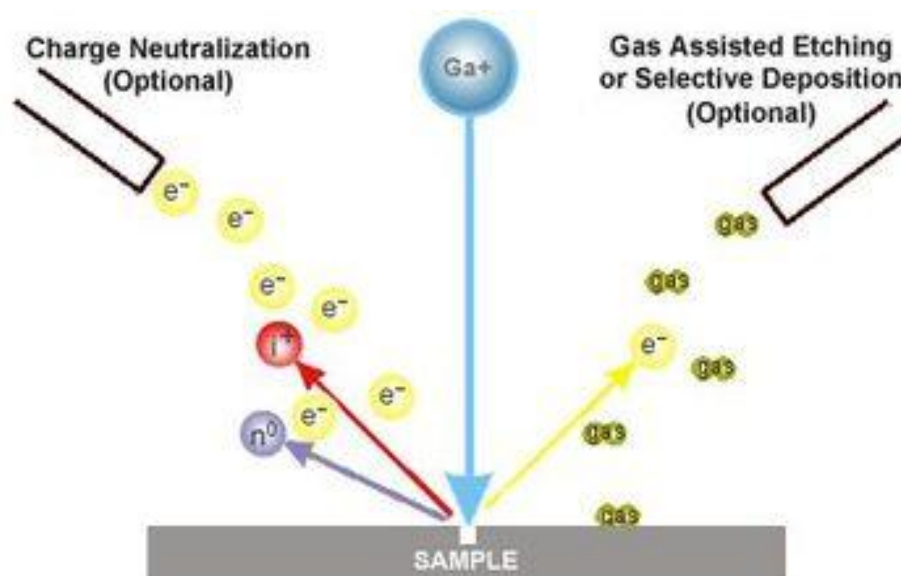

Figure 2.2: The principle of Focus Ion Beam milling.

The nanometre-scale resolution of FIB allows to mill the chosen exact region of interest is shown in Figure 2.3. The primary ion gallium hits the sample surface produces secondary electrons (e−). It sputters a small amount of material, which leaves the surface as either secondary ions (i^+ or i^-) or neutral atoms (n^0). The focused Ga-ion beam milling in a dual-beam apparatus to prepare the cross-sectional sample.

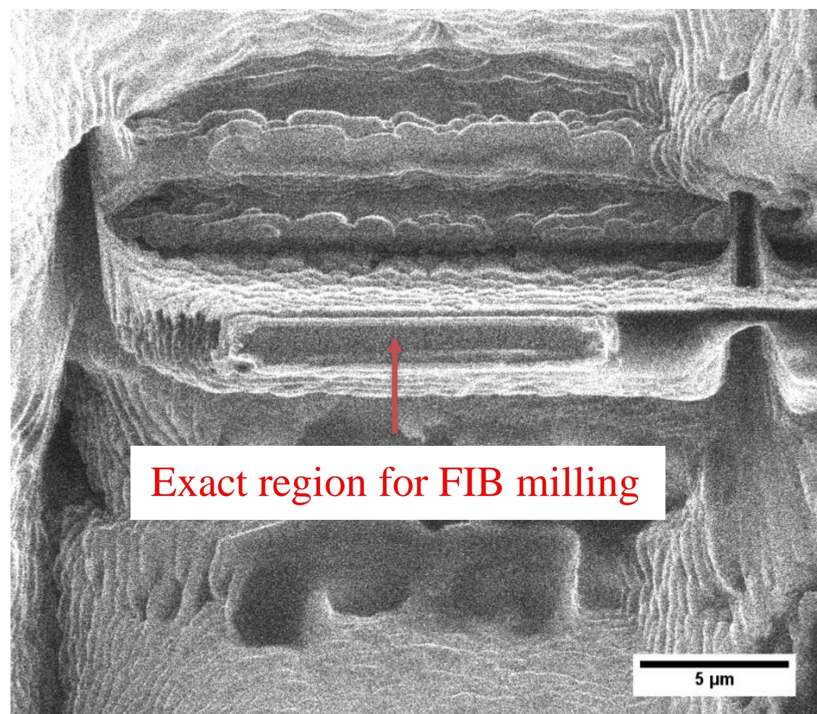

Figure 2.3: FIB milling Process

Before performing focused ion beam (FIB) milling, Platinum (Pt), Tungsten (W), and Carbon (C) protection layers on the IGZO thin film. First, in the FIB milling process, we milled both sides of the cross-sectional sample of the IGZO thin film down to a thickness of 1.0 µm at 30 kV and 1.0 nA. Second, this sample was thinned down to 0.5 µm at 30 kV and 0.5 nA. Third, the sample was milled down further to 0.3 µm at 30 kV and 0.3 nA. Finally, we performed FIB milling at 30 kV and 0.1 nA to obtain a cross-sectional sample with a thickness less than 50 nm. Figure 2.4 shows sample preparation process using FIB milling.

After the FIB milling processes, additional Ar ion milling was performed to remove the damaged layer formed on the sample surfaces by the Ga ion bombardment. Transmission electron microscopy (TEM) and scanning transmission electron microscopy (STEM) observations were performed using a Thermo Fisher Scientific Titan G2 60-300 (Thermo Fisher Scientific, USA) and JEOL ARM-200F (JEOL, Japan) electron microscope equipped with spherical aberration correctors.

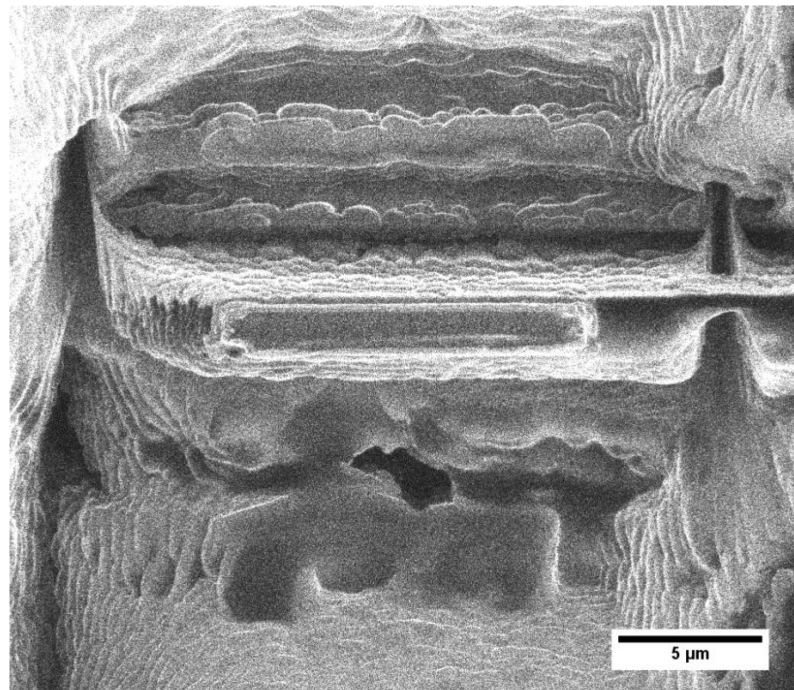

(a)

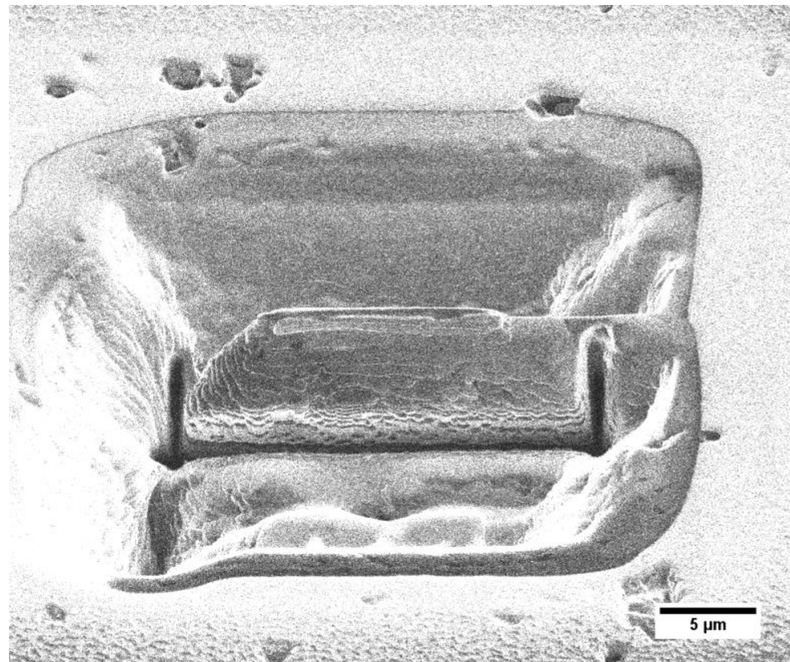

(b)

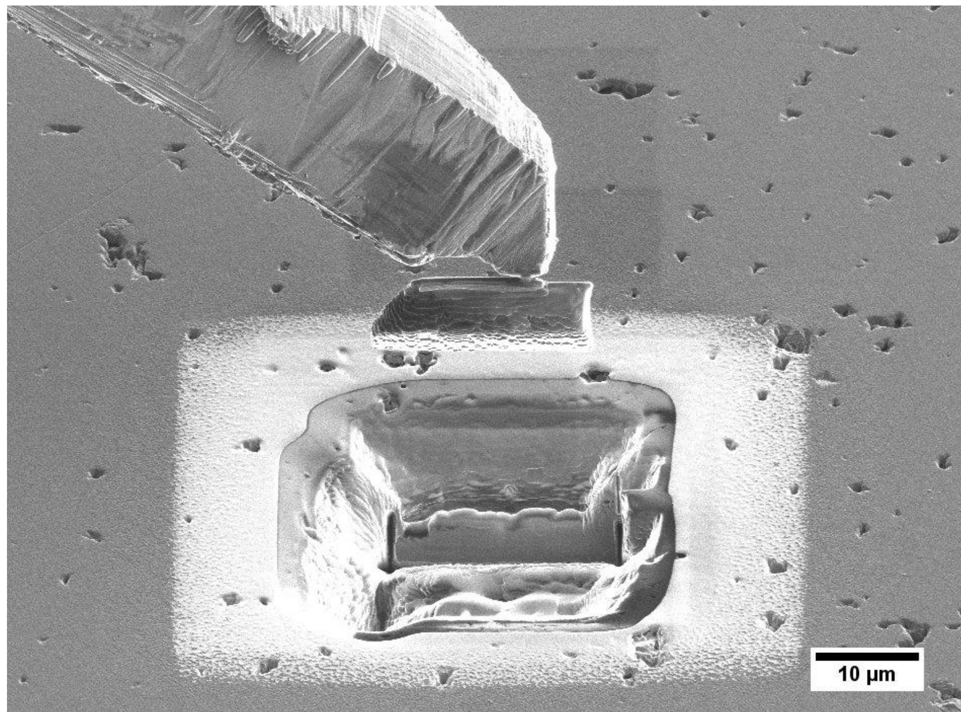

(c)

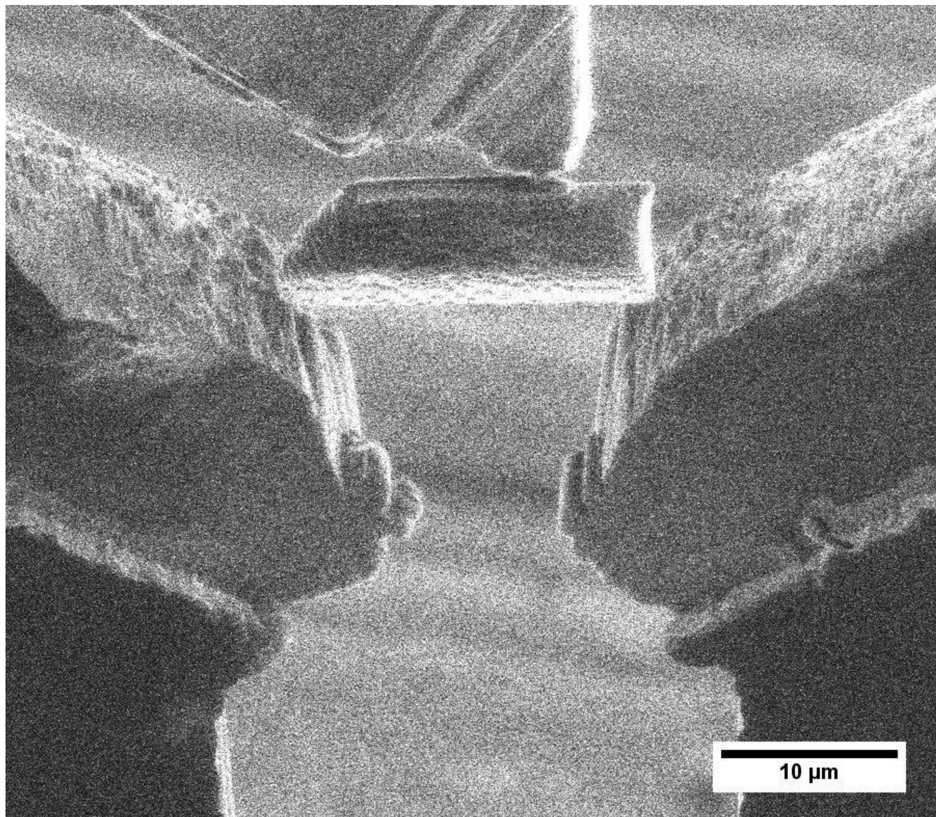

(d)

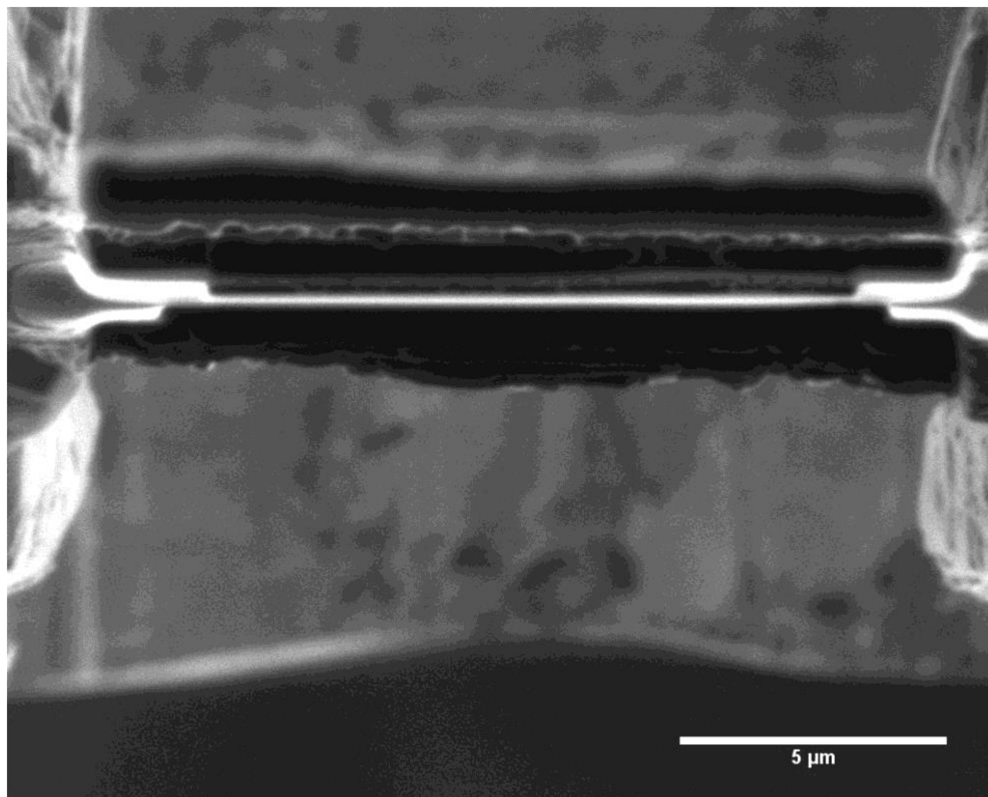

(e)

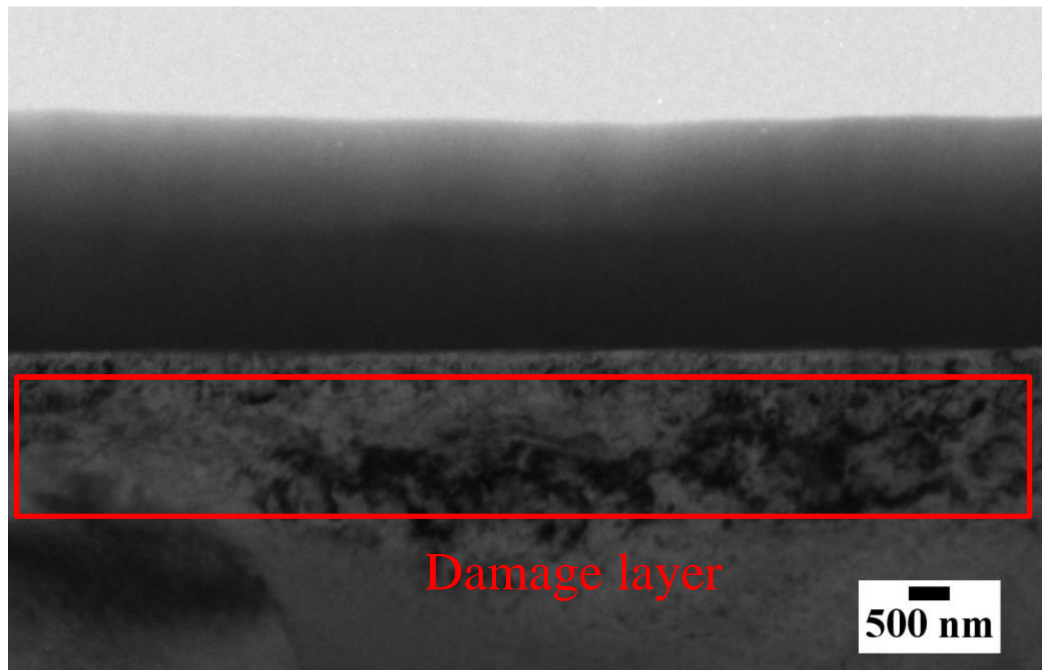

(f)

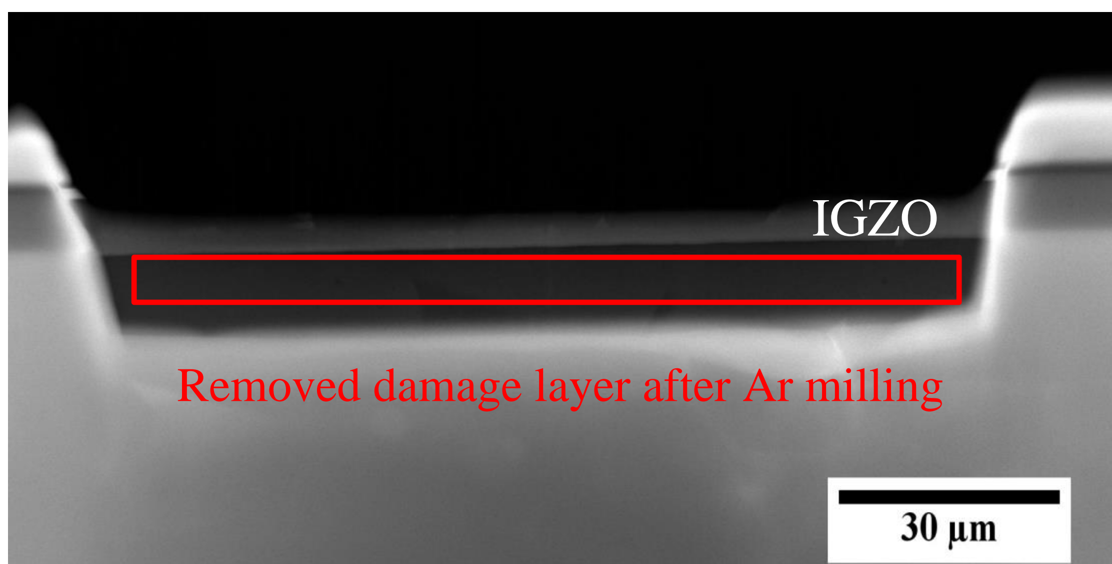

(g)

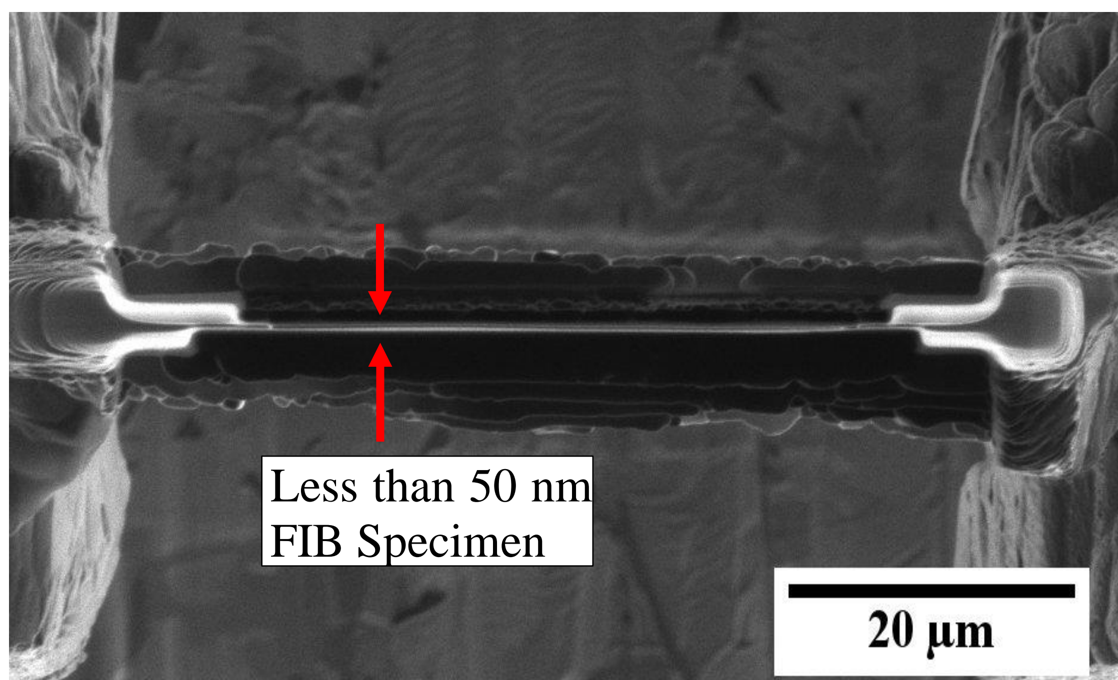

(h)

Figure 2.4: Sample Preparation using FIB milling (a)1st milling step, (b) 2nd milling step, (c) transfer the sample from specimen substrate using needle, (d) fixed on the sample holder (e) 3rd milling step, (f) 4th milling step (g) Bright-field (BF) transmission electron microscopy (TEM) image of a cross-sectional IGZO/α-Al2O3 film indicating Ga ion beam damage (red box), (g) a cross-sectional BF-TEM image after subsequent low-power Ar milling that effectively removed the damaged layer on the cross-sectional specimen (red box), and (h) a plan-view secondary-ion microscopy image of the thin foil specimen with a thickness less than 50 nm prepared by the Ga/Ar ion beam-milled Sample B.

2.3.2 Microstructure Analysis

The crystallinity of the IGZO thin films is verified using STEM observations. A typical result is shown in Figure 2.5. As shown in Figure 2.5 (a) and (b), the cross-sectional STEM images acquired from the different regions of the IGZO film show nano crystallinity. Herein, the IGZO specimen of less than 50 nm thickness was prepared by FIB. This shows the

imperfect crystallinity with local variations in lattice spacing. Because such areas with non-perfect crystallinity overlap with one another along the electron beam direction, it is challenging to directly visualize the local crystallinity. Nevertheless, certain areas showed evident lattice fringes in the amorphous matrix. The selected area electron diffraction pattern in Figure 2.6 (a) and (b) exhibits certain intensity maxima on the Debye ring. This feature strongly supports the formation of nanocrystals in the IGZO films. From the real and reciprocal space data, it is interpreted that (i) the average crystalline grain size is approximately 2–5 nm and (ii) the most common lattice spacing is approximately 0.24 nm to o.26 nm [Figure 2.7 (a) and (b)].

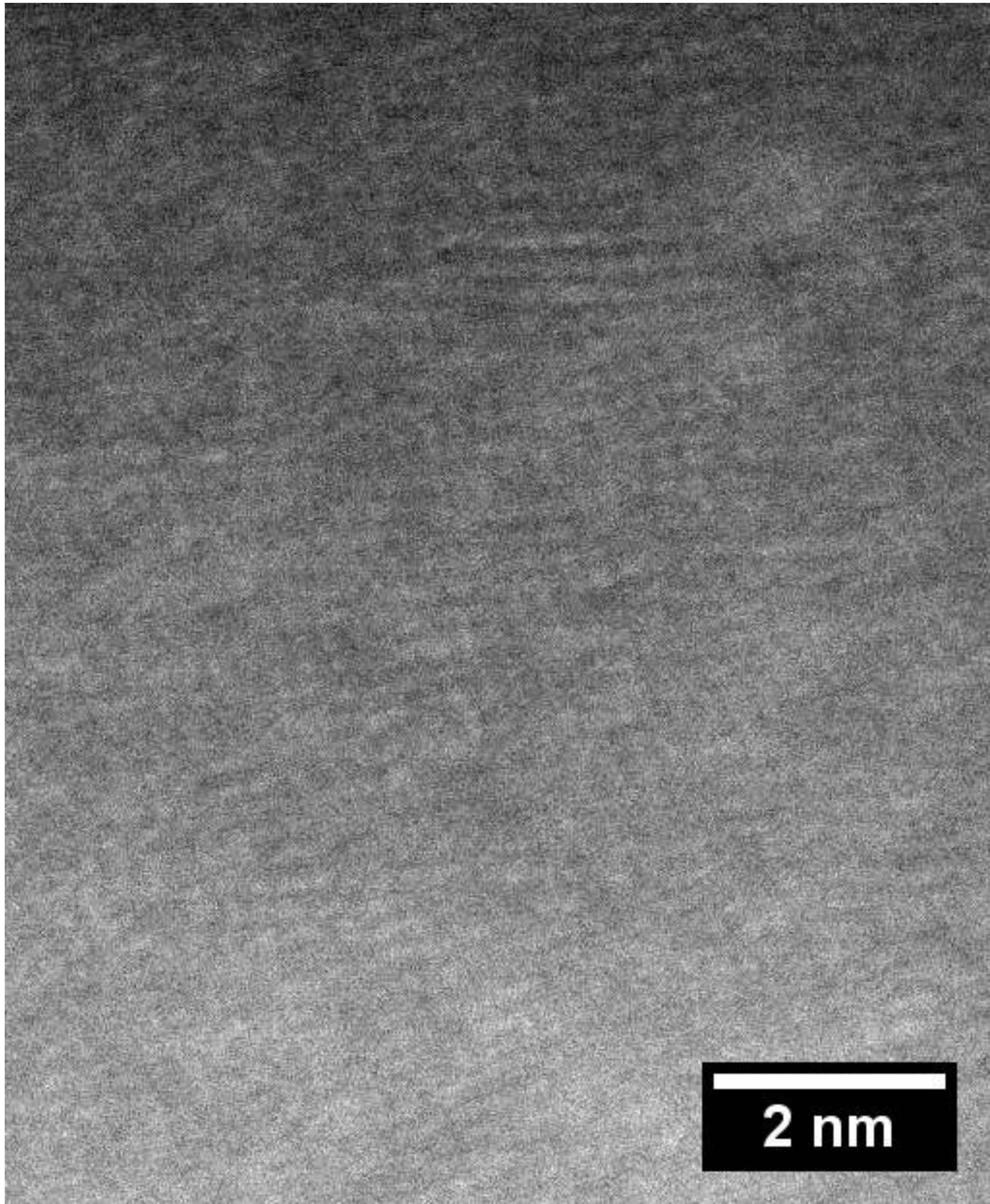

(a)

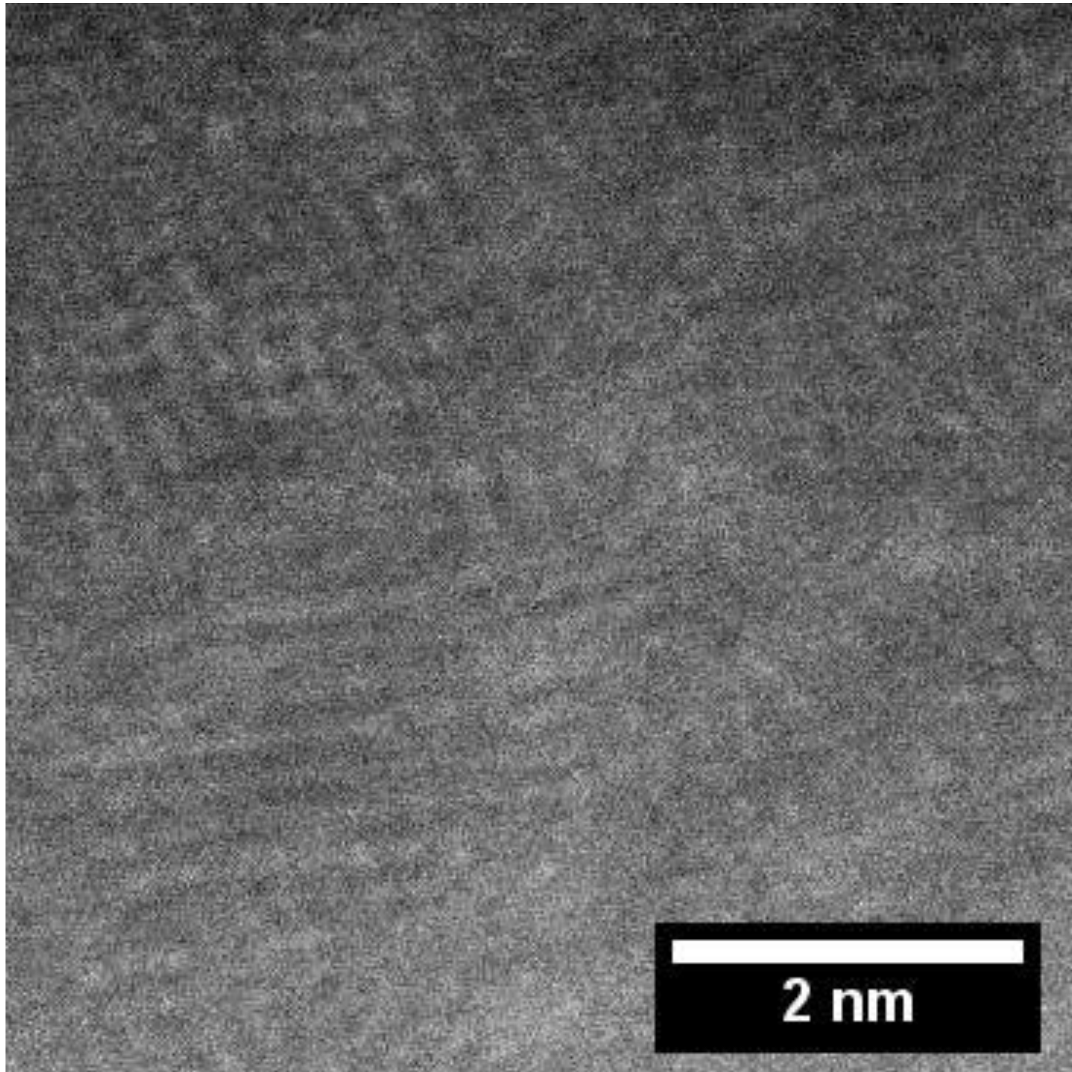

(b)

Figure 2.5: Cross-sectional scanning transmission electron microscopy (STEM) observation of Sample B. (a) and (b)Annular dark-Field (ADF) STEM image in different position.

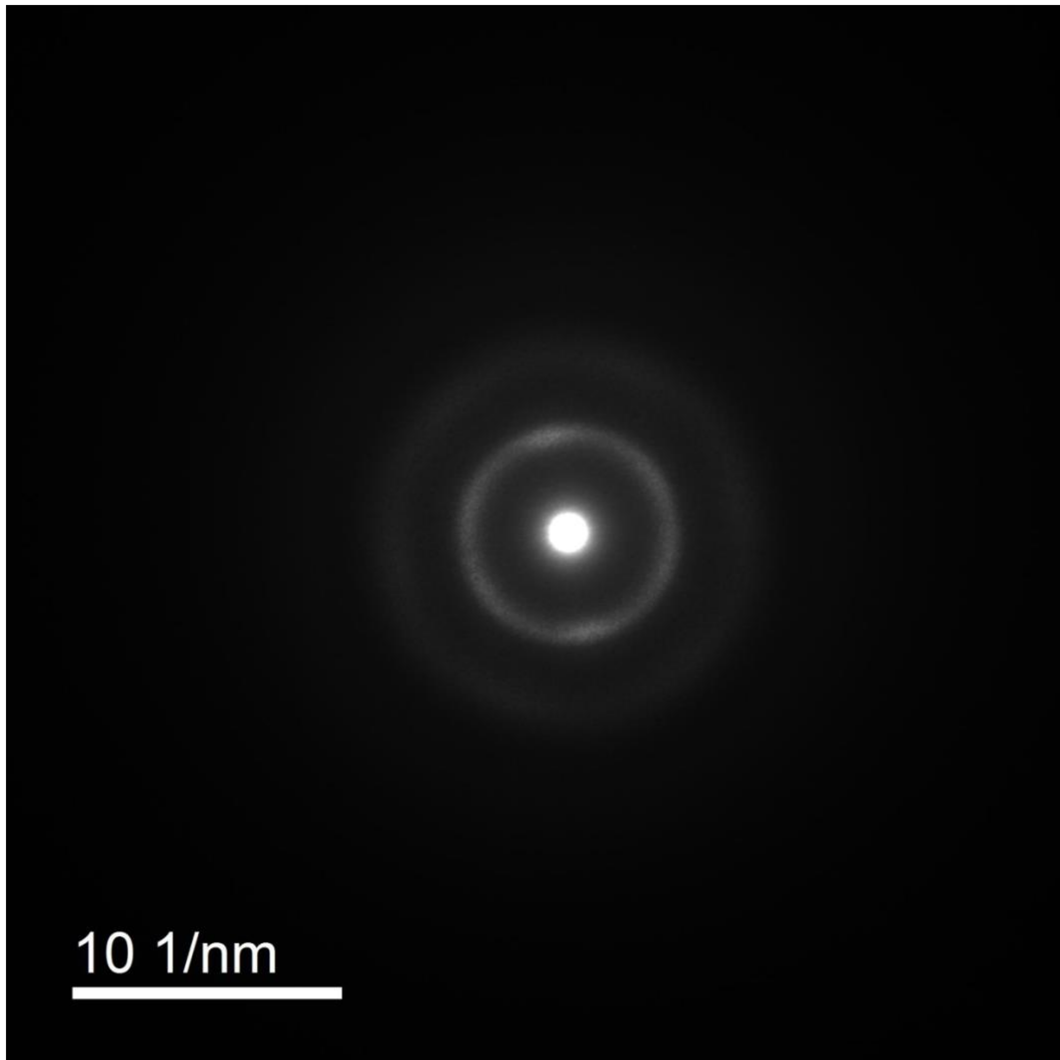

(a)

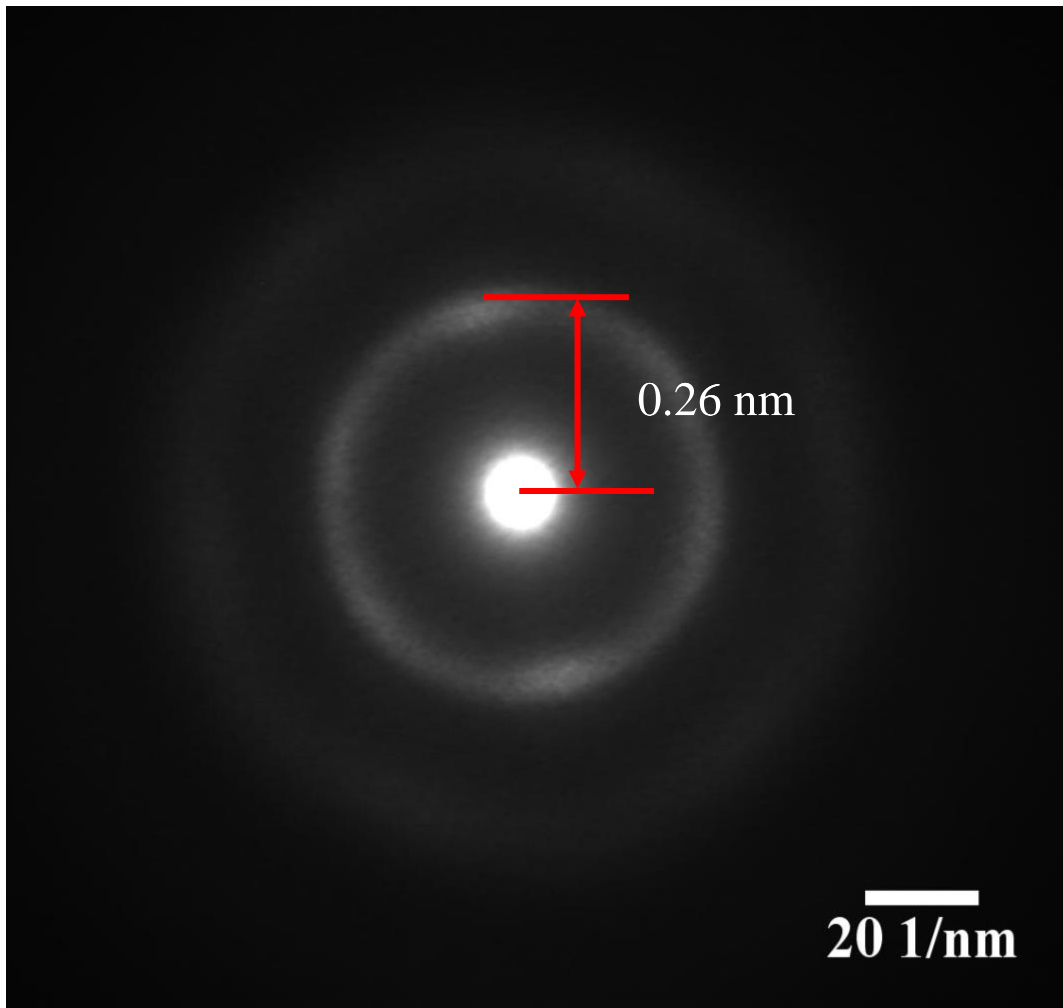

(b)

Figure 2.6: (a) and (b) selective area diffraction pattern acquired from the IGZO film under the TEM (parallel beam) mode at different region of specimen.

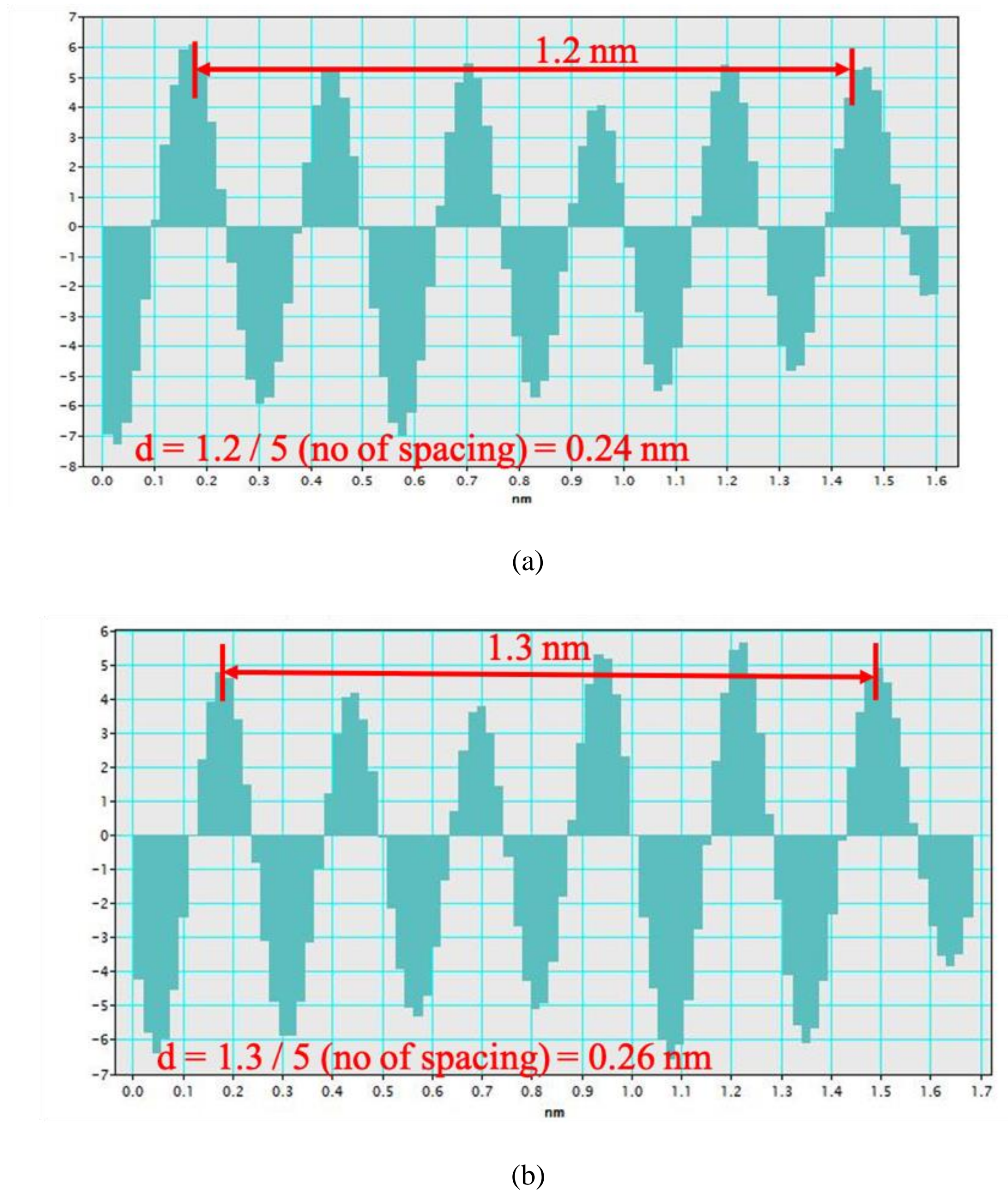

(a)

(b)

Figure 2.7 (a) and (b) lattice distance in two different regions

2.4 Conclusion

Electron microscopy observations revealed the presence of nanocrystals embedded in the amorphous matrix of the IGZO films. The annular dark-field (ADF) STEM observations revealed that nanosized crystals with an average crystal size of 2–5 nm and a lattice distance of approximately 0.24 nm to 0.26 nm were formed in the amorphous matrix of the fabricated IGZO thin films.

Chapter 3

Overview of the Thermal Conductivity Characterization Techniques for Thin Films

---

The knowledge of the thermal conductivity is used in a wide range of the applications in device application, photonics, microelectromechanical system (MEMS) and thermoelectric [17–19]. The thermal conductivity measurement technique for thin film has been developed significantly in last 20 years [20][21]. Despite these advancements, the thermal conductivity characterization of thin films remains a difficult task. In direct thermal conductivity measurement method, heat flux and the temperature difference between two points of the sample has required to determine. There are two types of measurement method for direct thermal conductivity measurement of thin film.

1. In-Plane thermal conductivity measurement
2. Cross-plane thermal conductivity measurement.

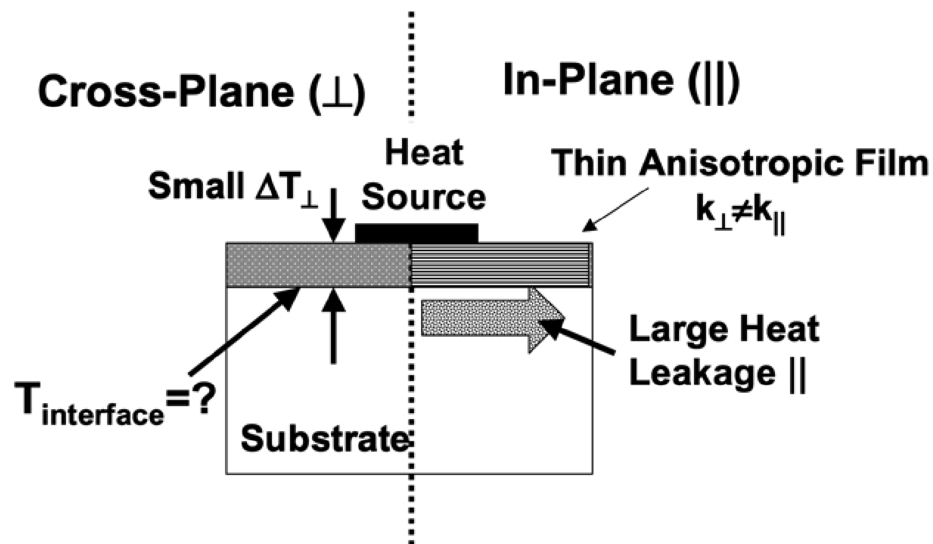

Figure 3.1: Sample configuration and challenges of the characterization [22].

Figure 3.1 shows the typical thin film sample configuration and the experimental difficulties with the thermal transport analysis of thin film on the substrate. To obtain the cross-plane thermal conductivity, it is required to measure the temperature drop across the film thickness. The challenge comprises two factors. first, reasonable temperature drop is created without creating large temperature rise in the substrate. Secondly, it is very difficult to experimentally measure the temperature drop across the thin film. The key problem of the in-plane measurement is the heat leakage through the substrate. For this reason, it is very difficult to measure the actual heat flow in the plane of the thin film, whose thickness is from nanometres to microns.

The cross-plane thermal conductivity measurement can be divided into two methods, such as,

I. The Three-Omega (3ω) Method

II. Steady-state Method

To avoid in-plane thermal conductivity measurement problems, there are three types of method, such as,

I. Membrane Method

II. Bridge Method, and

III. Heat spreading method

In these sections, each of the mentioned methods are generally explained to choose the suitable measurement technique for thermal conductivity measurement of IGZO thin films.

3.1 Electrical heating and sensing techniques

Electrical heating and sensing techniques are used to obtain the thermal conductivity characterization of thin films. Some methods employed the heaters also as a temperature sensor. In other techniques, separate heater and sensors are used. The electrical heating and sensing technique is better than optical heating and sensing technique because the heat transfer into the sample is possible to control. For this reason, it is possible to determine the temperature rise clearly. So that it is easier to measure the thermal conductivity directly. Sometimes, micro-heaters and micro-sensors are used to create high heat flux and temperature rise is possible to measure in micron scale. In cross-plane method, the strategies are measuring the surface temperature of the sample rather than the temperature drop by creating a large heat flux through the thin film while the substrate heat flux is minimized. Figure 3.2 shows the cross-plane thermal conductivity measurement strategy.

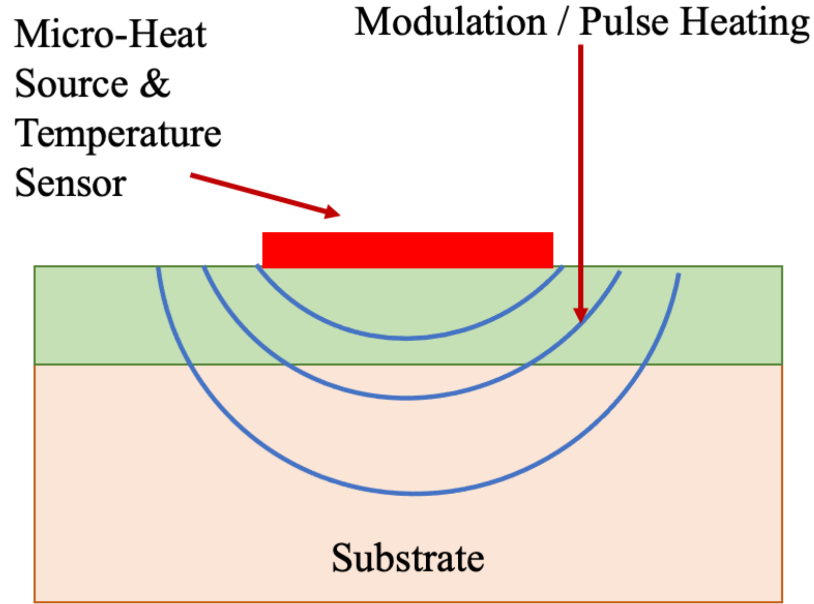

Figure 3.2: Cross-plane thermal conductivity characterization strategy.

3.2 Cross-plane thermal conductivity measurement of thin-film

3.2.1 The Three – Omega (3ω) Method

In the Three-Omega (3ω) method, a thin metallic strip is deposited on the sample surface which is act as a temperature heater and temperature sensors. An alternating current (AC), with angular frequency (ω) and amplitude I_o passing through the metallic strip. According to joule heating, the strip generates a heating source with power,

$$\text{Ac current,} \quad I(t) = I_o \cos(\omega t) \tag{3.1}$$

$$P(t) = I_o^2 R_h cos^2(\omega t) = \left(\frac{I_o^2 R_h}{2}\right)_{DC} + \left(\frac{I_o^2 R_h \cos(2\omega t)}{2}\right)_{2\omega} \tag{3.2}$$

Where R_h is the resistance of the metallic strip under the experimental condition. The temperature rise of the sample is also a superposition of DC component and 2ω AC component:

$$T(t) = T_{DC} + T_{2\omega} \cos(2\omega t + \varphi) \tag{3.3}$$

Here, $T_{2\omega}$ is the amplitude of the AC temperature rise and φ is the phase shift induced by the thermal mass of the system. The resistance of the heater will change with 2ω variation if the resistance of heater depends lineally on temperature. So the resistance of the metallic strip is,

$$R_h(t) = R_o[1 + C_{rt}\{T_{DC} + T_{2\omega}\cos(2\omega t + \varphi)\}]$$
$$= R_o(1 + C_{rt}T_{DC})_{DC} + (R_o C_{rt} T_{2\omega}\cos(2\omega t + \varphi))_{2\omega} \quad (3.4)$$

Where C_{rt} is the temperature coefficient of the resistance (TCR) of the heater and R_o is the heater resistance at room temperature. The voltage drop across the strip can be calculated by multiplying current (3.1) and the resistance (3.2):

$$V(t) = I(t)R_h(t)$$
$$= [I_o R_o(1 + C_{rt}T_{DC})\cos(\omega t)]_{power_{source}} + \left(\frac{I_o R_o C_{rt} T_{2\omega}}{2}\cos(3\omega t + \varphi)\right)_{3\omega}$$

$$+ \left(\frac{I_o R_o C_{rt} T_{2\omega}}{2}\cos(\omega t + \varphi)\right)_{1\omega} \quad (3.5)$$

This expression contains the voltage drop of 1ω frequency based DC resistance of the heater and two new components which is proportional of the temperature rise in the heater, modulated at 1ω and 3ω frequencies, respectively. The 3ω voltage component is detected by lock-in-amplifier or LABVIEW digital to analog (D/A) converter to extract the temperature amplitude of the heater:

$$T_{2\omega} = \frac{2V_{3\omega}}{I_o R_o C_{rt}} \approx \frac{2V_{3\omega}}{V_{1\omega} C_{rt}} \quad (3.6)$$

The heat conduction model is used to obtain the thermal conductivity of substrate and thin film. The temperature amplitude of the heater can be written as,

$$T_{S+F} = T_S + \frac{\rho d_f}{2bwk_f} \quad (3.7)$$

Where b is the half-width of the heater, ρ/w is the power amplitude dissipated per unit length, d_f is the film thickness, k_f is the thermal conductivity of the thin film, and T_S is the temperature rise between the film and substrate. To determine the thin film thermal conductivity, the temperature between film and substrate is important to determine accurately. The way to estimate the temperature drop across the thin film is to infer it experimentally [23]. This technique measures the difference between the top surface temperature rise between the sample and the reference (only substrate). Figure 3.3 shows the schematic diagram and example of the method.

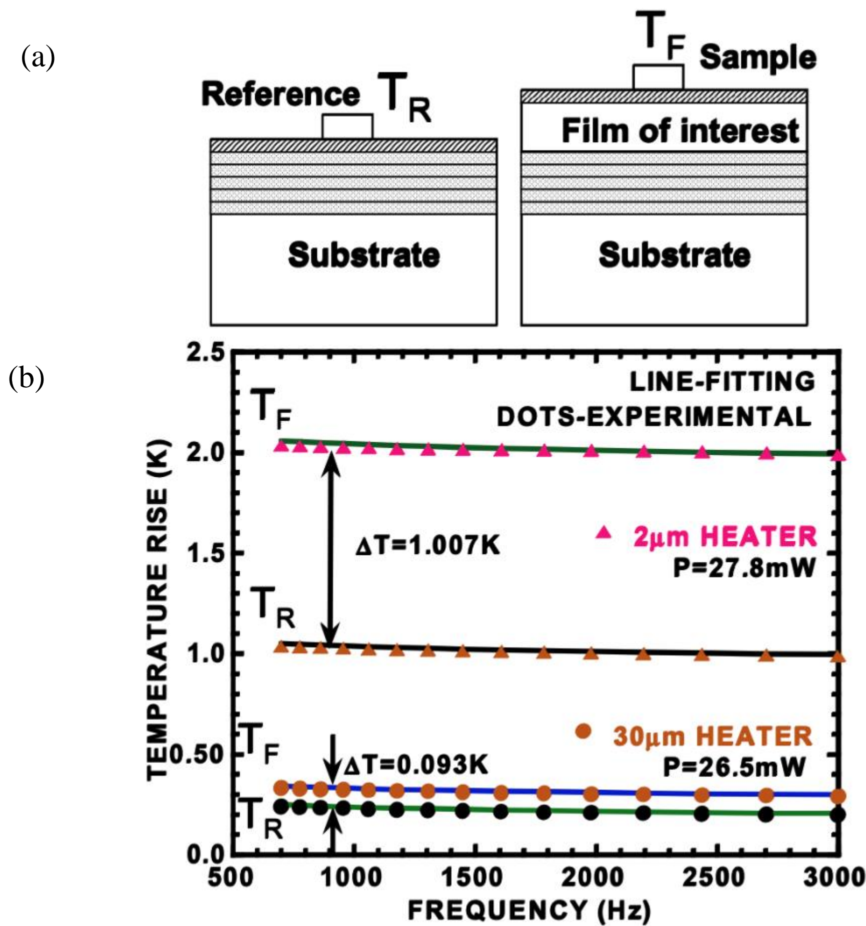

Figure 3.3: (a) Schematic diagram of sample and reference, (b) example of the experimental method [22].

3.2.2 Steady – State Method

A steady-state method has also employed to determine the cross-plane thermal conductivity of thin film and the thermal boundary resistance between the micron size heater/thermometer and the substrate [20][24]. In this method, at least two, and sometimes three, metallic strips are used to determine the temperature rise of thin film and reference. One stripe has a large width for the temperature rise of the film surface which is acting as a heater as well as thermometer. A second thermometer is placed nearness at a known distance to the heating strips, which provides the temperature rise of the substrate. Using the two-dimensional heat conduction model and a known thermal conductivity of the substrate, temperature rise of the substrate is possible to determine. If the substrate thermal conductivity is unknown, then a third thermometer is at the different position away from the heater is used to determine the substrate thermal conductivity. By depositing thermometer array onto the substrate, the thermal boundary resistance between the heater and the substrate is possible to measure. In conclusion, the 3ω method is easier than steady-state method.

3.3 In-plane thermal conductivity measurement of thin-film

The thermal conductivity measurement in-plane direction, often used the strategy to remove the substrate for the determination of the heat flux through the thin film. The structure of the film with a heater which is suspended from the substrate is called free-standing structure. Another technique is deposit thin film onto thin and low thermal conductivity sample which minimize the heat leakage. Another method sometime takes advantages of the lateral heat spreading at surrounds of the heater. Figure 3.4 shows the thermal conductivity characterization strategies in the in-plane direction.

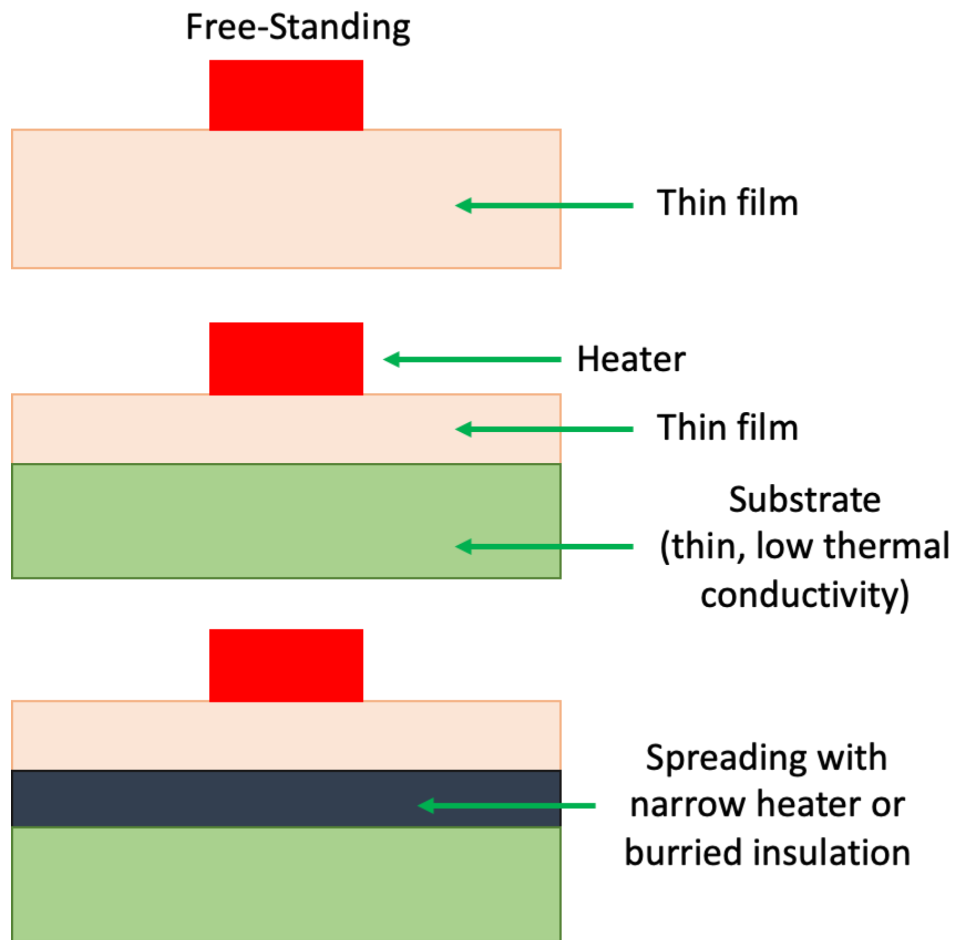

Figure 3.4: In-plane thermal conductivity measurement strategies

3.3.1 Membrane Method

There are two strategies have been developed for the thermal conductivity measurement of film using membrane method. One of the configurations of membrane structure is a suspended structure where the heater and thermometer are fabricated on a large membrane [25–29]. The membrane can be the film on a thin substrate structure which is suspended between massive heat sink [25]. Another way is to remove the substrate underneath the film, making the film as a free-standing structure. Figure 3.5 shows the configuration of membrane method. In both cases, the heat is generated through the heater and spreads from the middle of the membrane towards its edges. The heater detected the temperature profile. The thermal conductivity of the film can be determined as,

$$k = \frac{\rho L}{wd(T_h - T_s)} \tag{3.8}$$

Where ρ/w is power dissipation of the heater per unit length, L is the distance from heater to heat sink, T_h is the temperature rise of the heater, and T_s is the temperature of sink. The experiment should be carried out in a vacuum state.

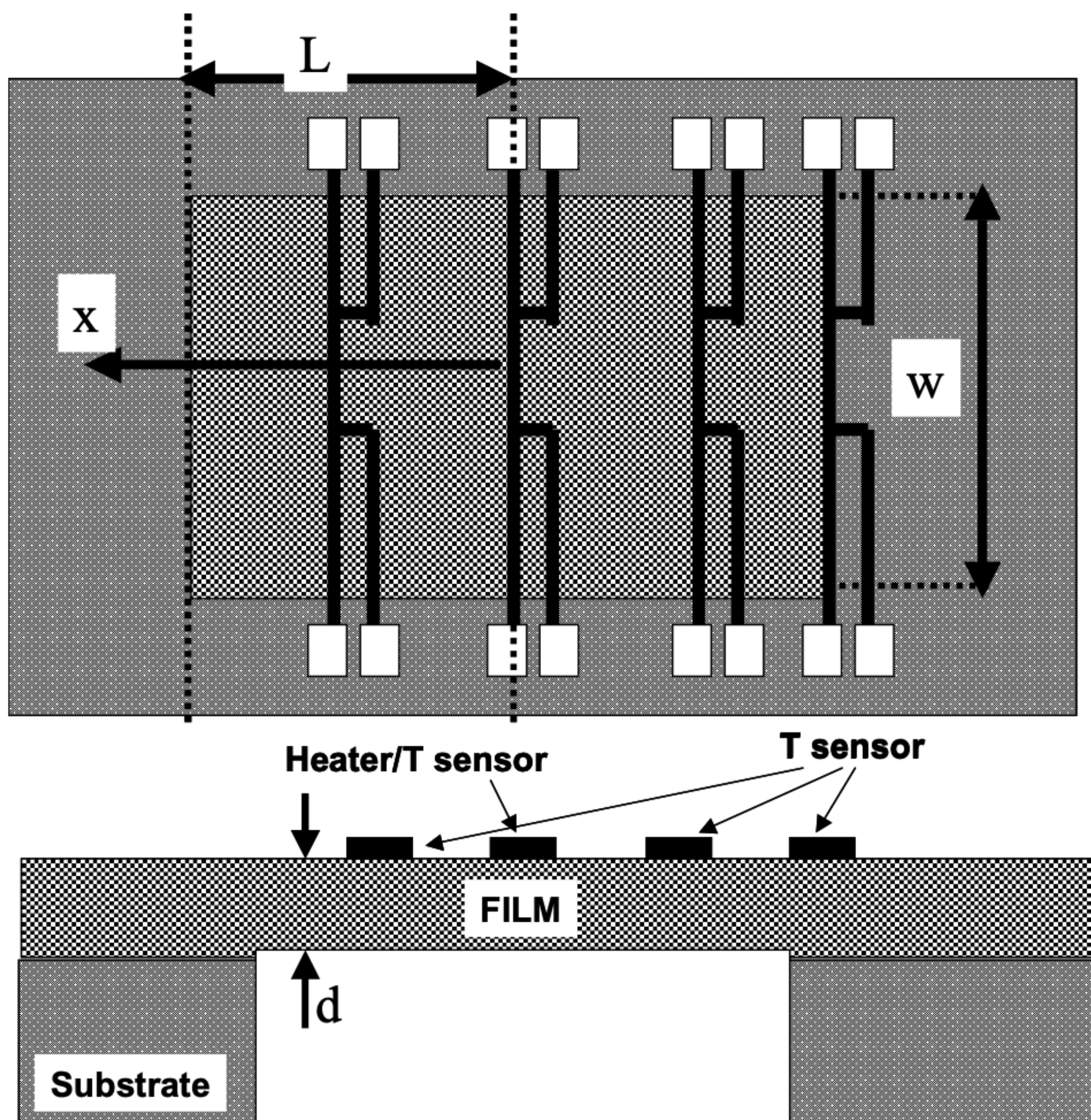

(a)

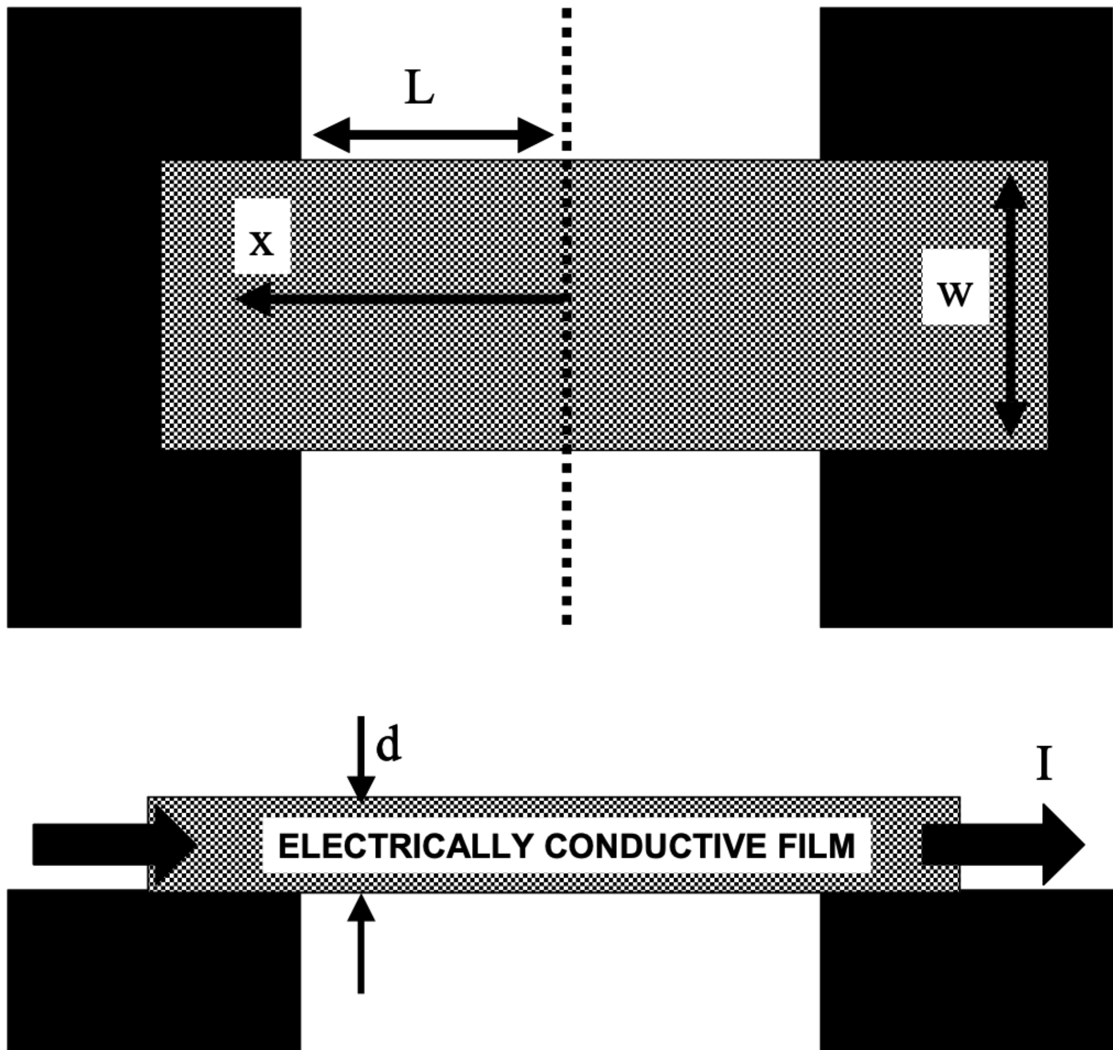

(b)

Thermal Insulation

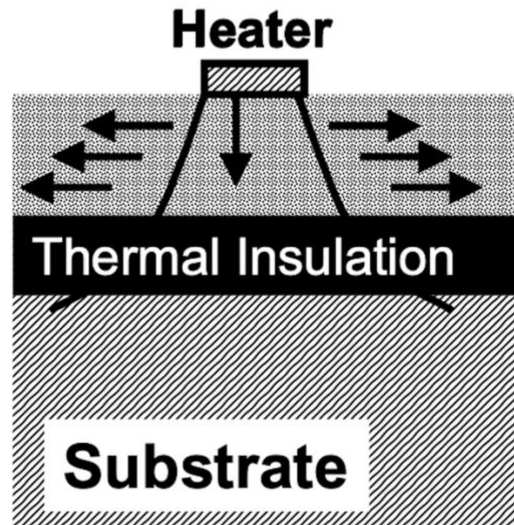

Narrow Heater

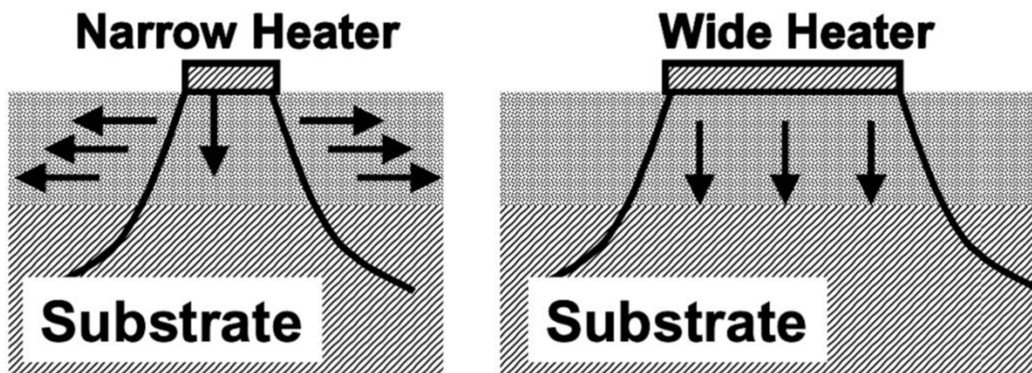

(c)

Figure 3.5: Important experimental methods for in-plane thermal conductivity characterization: (a) membrane method, (b) bridge method, and (c) in-plane heat spreading method using buried thermal barriers with narrow width wire [22].

3.3.2 Bridge Method

The principle of the bridge method for the in-plane thermal conductivity characterization is shown in Figure 3.5 (b). This method is only applies if a current can pass through pass through the film. If the film is insulating, then another conductive layer with known properties is needed to deposit onto film. The film is patterned as thin strip which makes a bridge between the gap of two heat sinks. The film itself acts as a heater and thermometer when an AC current passes through it. The temperature rise of the heater is determined by the change of its resistance. The experiments should be performed in vacuum ambient as membrane method to minimize the convection heat transfer effect.

3.3.3 Heat spreading Method

In this method, the film is deposited on thin and low thermal conductivity supporting films. General deposition process is not applicable, the film should be grown epitaxially. Figure 3.5 (c) shows the sample structure of the heat spreading method. Low thermal conductivity supporting film acts as a thermal insulation. A heating strip is deposited onto the film surface, which is act as a heater [30]. When an AC current passes through the heater, the temperature rise is sensitive to the in-plane thermal conductivity of the film. Ju et al. reported that the steady-state temperature distribution in the film plane is determined by electrical resistance thermometry in heater strip at different distance to the heat source [31]. The thermal conductivity of film can be determined from the experimental temperature rise and input power. The model considers the heat conduction across the thermal insulating layer to the substrate and along the film.

Chapter 4

Temperature Dependence Thermal Conductivity of IGZO Thin Films

Indium–Gallium–Zinc-Oxide (IGZO) thin-film transistors (TFTs) have attracted considerable research attention in the area of TFT technology. Their electronic device applications are being enhanced owing to their remarkable performance, e.g., high electron carrier mobility, better uniformity over a large area, and potential optical transparency [3]. Moreover, IGZO can be a promising thermoelectric candidate for its comparable thermoelectric performance to other oxide candidates [12]. The thermal conductivity of IGZO indicates its ability for heat conduction, which is subject to various factors, and can be subdivided into electro- and phono-thermal conductivities revealed by phonon–phonon and electron–electron scattering [32]. The thermal properties of IGZO thin films are also of vital importance for heat dissipation and thermal management of devices. Although the atomic-scale structure of IGZO films is unclear whether these are amorphous or crystalline [33–35]. Regardless of various studies on thermoelectric properties of IGZO thin film, there are no significant studies which on the relation between temperature dependence thermal conductivity and microstructure analysis. Consequently, first this chapter presents the fabrication process and conditions of IGZO thin films. Secondly, this chapter includes the temperature dependence thermal conductivity characterization of the Indium–Gallium–Zinc–Oxide (IGZO) thin films with the differential three-omega (3ω) method. Thirdly, instead of

temperature dependence thermal conductivity results analysis, the phonon mean free path is estimated. Finally, this chapter includes the circumstantial conclusion of this research.

Sample Preparation for 3ω measurement

A 500 nm IGZO (In:Ga:Zn = 1:1:1) thin films with were deposited on an alumina substrate by DC magnetron sputtering method at room temperature. The deposition rate (2.5 nm/min) of this method is higher than others, such as pulsed laser deposition (PLD), radio frequency (RF) sputtering [36]. A mixture of Ar and O_2 gas was used during the sputtering process. The oxygen partial pressure [PO_2] was calculated from the ratio of O_2 gas flow rate and total Ar/O_2 flow rates. Three samples at various [PO_2] such as [PO_2] = 0 % (Sample A), [PO_2] = 10 % (Sample B, and [PO_2] = 65 % (Sample C) were deposited to pursue the measurement. Figure 4.1 shows a plan view of the dimension of shadow mask and a cross-sectional view of the film samples and reference. A 30 nm aluminum wire strip is deposited on the IGZO thin film in vacuum using 30 μm width and 2 mm length shadow mask for three-omega measurements [37].

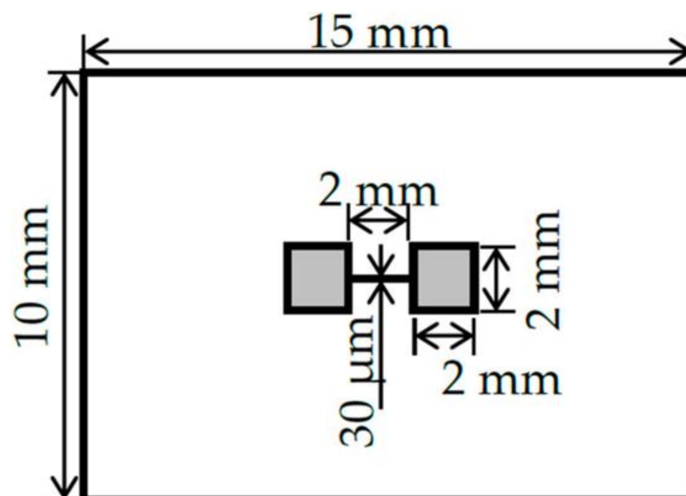

(a)

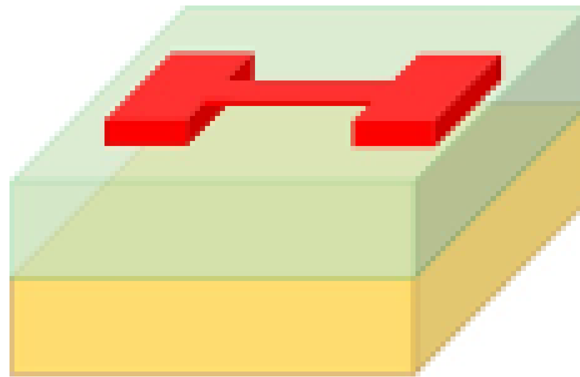

(b)

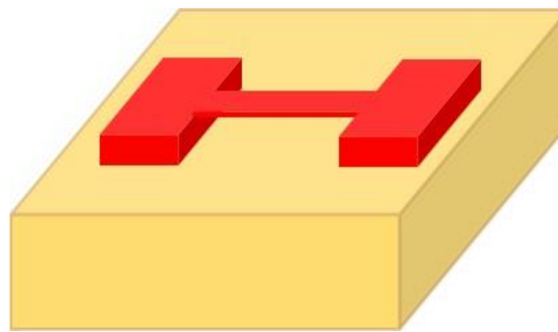

(c)

Figure 4.1: Plan view of the shadow mask of the heater with the length of 15 mm, width of 10 mm and a thickness of 20 μm (a) and the schematic diagram of a film sample (b) and the reference (c).

4.1 Temperature Dependence Thermal Conductivity Measurement Using 3ω Method

The 3ω method is a highly simple, accurate and effective thermal conductivity measuring technique of thin films and bulk materials [38][39]. In this method, an insulating thin layer is required between aluminium thin wire and IGZO thin film to prevent the current flow through the sample and substrate. The aluminium wire strip act as a heater and thermometer at the same time. An alternating current (AC) was applied through the

aluminium wire strip with an angular frequency of ω. Furthermore, a 10 Ω shunt resistance was connected in series to acquire the reference signal at a frequency of ω. The metallic wire strip was Joule heated at a frequency 2ω, of according to $P = I^2R$. The metallic resistance temperature coefficient, (1 / R) (dR / dT), was measured by heating the sample. With the application of an AC at ω, voltage oscillation at a frequency of 3ω (denoted as $V_{3\omega}$) could be observed. The temperature oscillation ($T_{2\omega}$) at the frequency of 2ω, expressed as

$$T_{2\omega} = 2\frac{dT}{dR} \cdot \frac{R}{V_{1\omega}} \cdot V_{3\omega} \tag{4.1}$$

The electrical resistance is proportional to the temperature. For this reason, the temperature is also fluctuated at 2ω due to Joule heating at 2ω. The metallic wire resistance was varied with the oscillation at 2ω, i.e., $T_{2\omega}$. The thermal conductivity of the thin film, K_f, can be expressed as follows:

$$\kappa_f = \frac{Pd_f}{wl\Delta T_{2\omega,f}} \tag{4.2}$$

where P is the AC heating power, df is the thickness of the film, w is the width, and l is the length of the wire strip. A 16-bit digital-analog converter and LabVIEW® system were functioned to track the 3ω signal. The 3ω is ten thousand times smaller than that of the ω voltage signal and it is possible to measured even at an intensity. The thermal conductivity of various temperature was also measured from room temperature to 373 K. To determine the thin film thermal conductivity, the temperature between film and substrate is important to determine accurately. The way to estimate the experimentally temperature drop across the

thin film is to infer it. Figure 4.2 shows the temperature oscillation (1 / R) (dR/dT) across the IGZO thin film ($T_{2\omega}$, f) at the frequency of 2ω. The difference between the top surface temperature rise between the sample and the reference (only substrate) is measured from the experimental values of temperature oscillation with increasing of frequency.

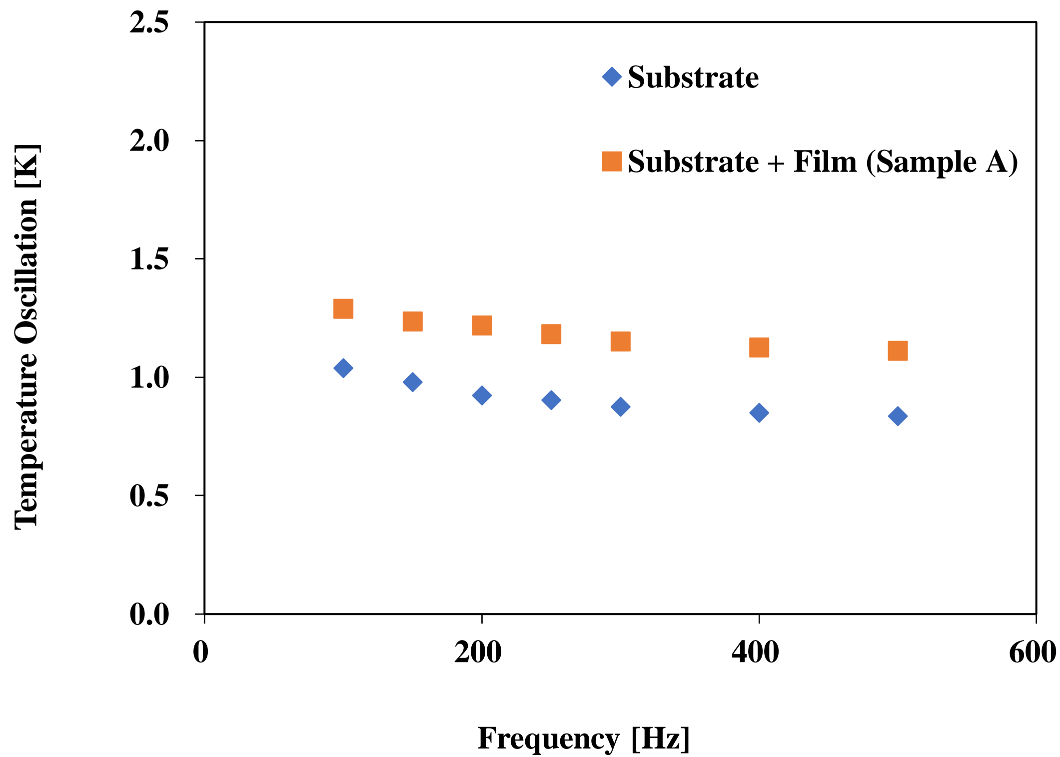

(a)

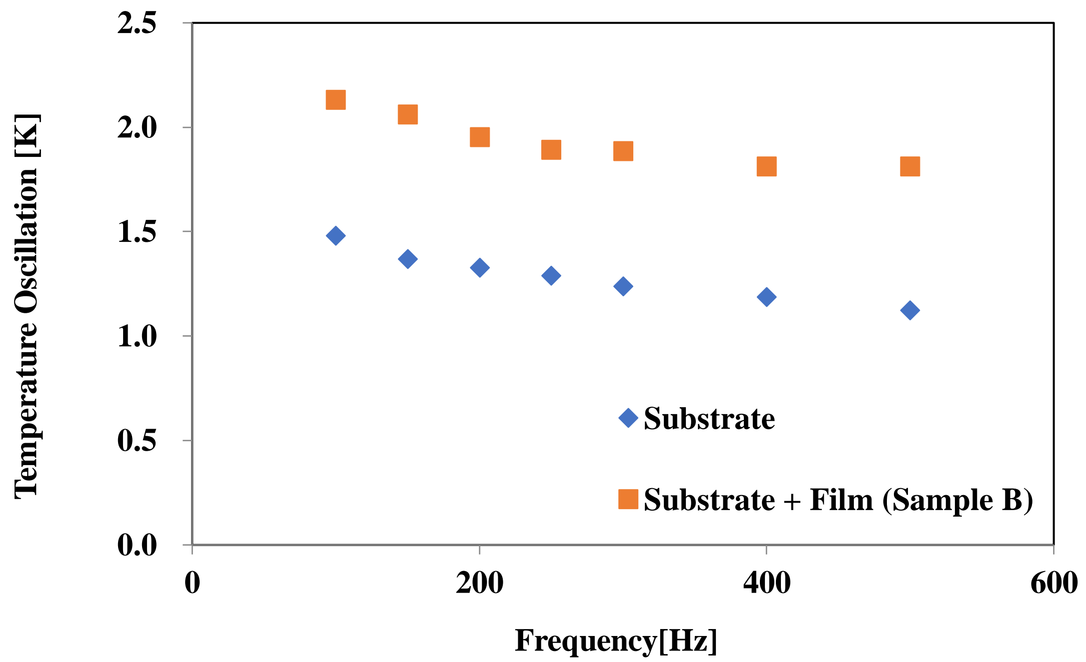

(b)

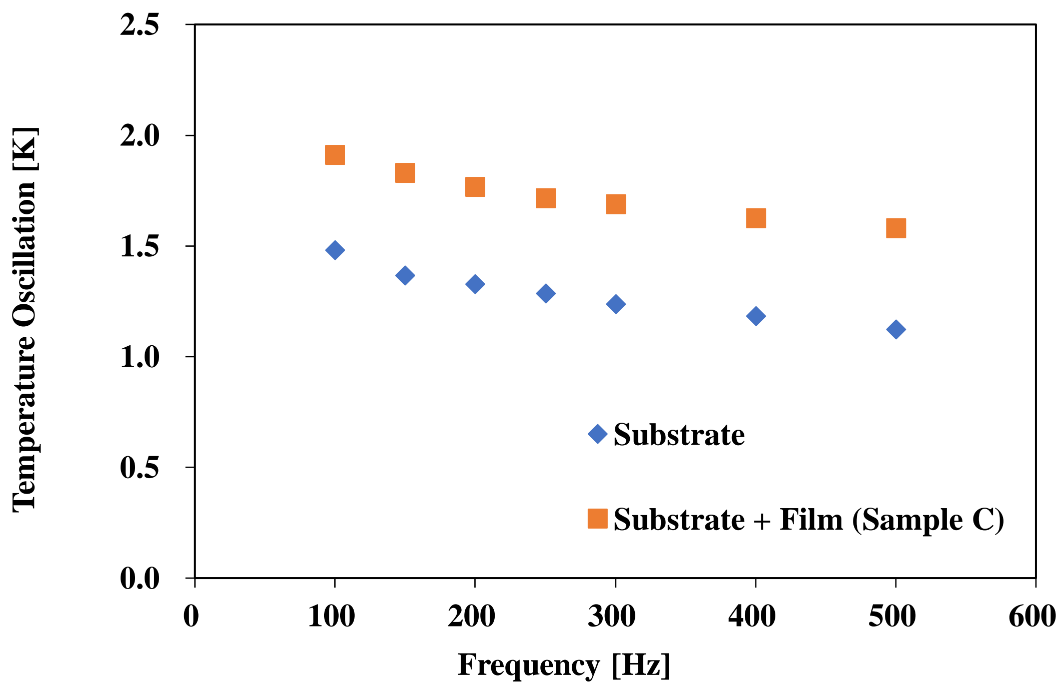

(c)

Figure 4.2: Temperature oscillation Amplitude of (a) Sample A, (b) Sample B, and (c) Sample C at room temperature.

The thermal conductivity values of Samples A, B, and C at room temperature are 1.65, 1.76, and 2.58 W m $^{-1}$K^{-1}, respectively. The thermal conductivity of samples B and C is higher than sample A because of higher oxygen partial pressure of IGZO thin films. Oxygen partial pressure is directly associated with the oxygen vaccancies. Figure 4.3 shows the thermal conductivity values of samples A, B, and C at different temperatures. It is clearly revealed that the thermal conductivity decreased with an increase in temperature. This temperature dependence is similar to that for crystalline materials because the thermal conductivity of amorphous materials increases with an increase in temperature in the room-temperature region [40–43]. The thermal conductivity is directly associated with the mean free path and have proportional relationship. The phonon mean free path of all amorphous materials is shorter than crystalline materials.

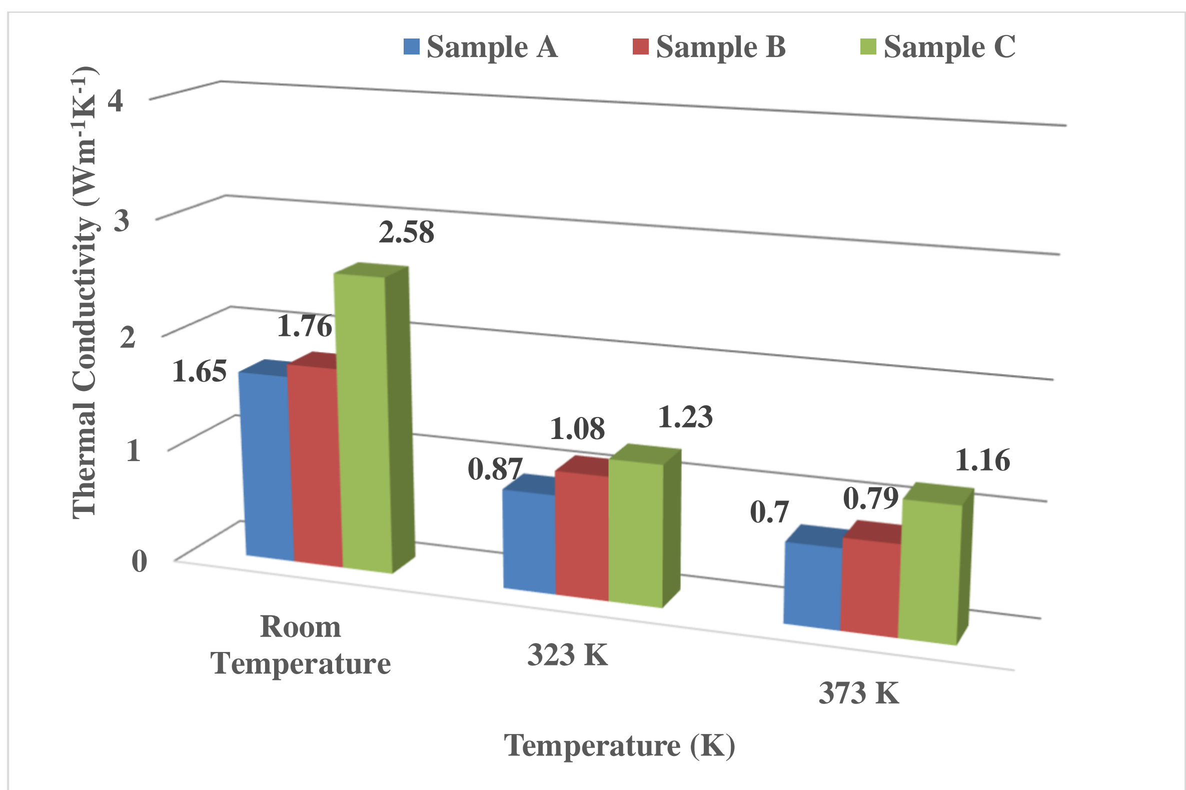

Figure 4.3: Temperature dependence of thermal conductivity of IGZO thin films in the temperature range from room temperature to 373 K.

4.2 Estimation of Mean-Free Path

Heat conduction in solids is possible to explain using the phonon-phonon interaction phenomenon. The thermal conductivity of phonon can be described according to the phonon gas model, can be expressed using the following equation:

$$k = \frac{1}{3} C_v v l \tag{4.3}$$

Where k is the thermal conductivity of phonon, C_v, v and l are the specific heat capacity, average phonon velocity, and phonon mean free path, respectively. The specific heat capacity of the thin film may be fixed and not dependent on the film thickness or chemical composition. The average phonon velocity (v) can be assumed as the sound velocity, which is calculated using the following equation:

$$v = \sqrt{\frac{E}{\rho_d}}. \tag{4.4}$$

Where E is Young's modulus and ρ_d is the film density. Film density may vary depending on film thickness or deposition condition, but it is negligible. The thermal conductivity directly dependent on the mean free path, so that it is a very important parameter. Figure 6 shows the values of Young's modulus, which is measured by the nano-indentation method at various indentation depths. Although it is not evident why the measured values increase with the indentation depth, the average Young's modulus of the IGZO films can be determined around 200 GPa from a narrow plateau at the indentation

depth of 100 nm. The Young's modulus and the phonon velocity are constant across the sample. The density and specific heat capacity of the IGZO films are reported to be 5.86 g.cm–3 and 426 $Jkg^{-1}K^{-1}$[43].

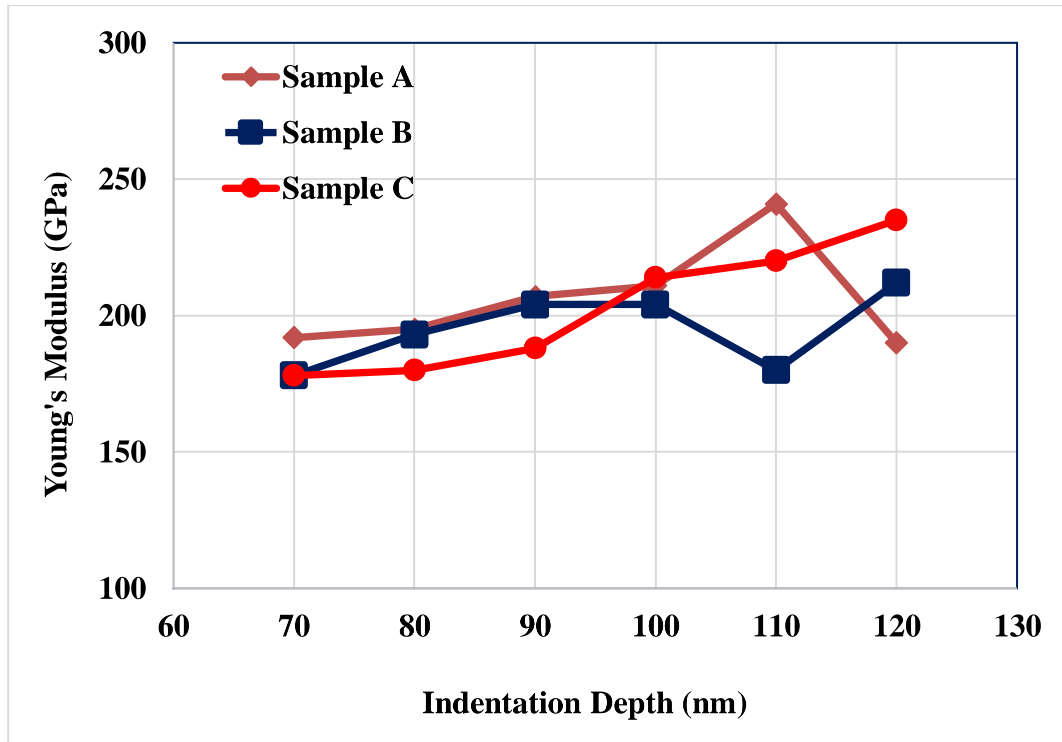

Figure 4.4: Young's modulus with various indentation depths of 500 nm IGZO thin films

The phonon mean free paths were estimated at room temperature using equations $k = \frac{1}{3}C_v vl$ (4.3) and $v = \sqrt{\frac{E}{\rho_d}}$.

(4.4), which are very narrow around the nanometer range. In Figure 4.3, the thermal conductivity of $[PO_2]$ = 65 % (Sample C) is higher than those of $[PO_2]$ = 0 % (Samples A) and $[PO_2]$ = 10 % (Sample B). This indicates that the phonon mean free path of $[PO_2]$ = 65 % (Sample C) is longer than others. The thermal conductivity is decreasing with an increase in temperature because the phonon-phono scattering is increasing with an increase in

temperature. This phenomenon is a common feature for all crystalline materials. The mean free path has an inverse proportional relationship with the temperature. Hence, the thermal conductivity of T^{-1} dependence is negligible in amorphous materials (glass) significant in crystal. At low temperatures, the mean free path is intrinsically short owing to the short-range order atomic arrangement . Therefore, the temperature dependent thermal conductivity of IGZO thin films shown in Figure 4.3 indicates a clear demonstration of the significant crystallinity.

4.3 Conclusions

The temperature dependence thermal conductivity of the IGZO thin films clearly demonstration the presence of nano-crystallinity. The thermal conductivities decreased with increase in the ambient measurement temperature is similar thermal property to that of crystalline materials. This study clearly states a relationship between microstructure analysis and thermal conductivity characterization.

Chapter 5

Application of Indium Gallium Zinc Oxide (IGZO) Thin Film Transistor Application

5.1 Overview of Indium Gallium Zinc Oxide TFTs

In 1792, Alessandro Volta first introduced the term “semiconducting” [44]. After that, the semiconductor materials and devices started to change the world beyond its expectation. The history of semiconductors really dates to 1833, when Michael Faraday scientifically observed experimentally the effect of electrical conductivity of silver sulphide increased with increasing temperature [45]. Based on the understanding of a metal-semiconductor contact i.e. Schottky diode, in 1939 [46], Shockley invented an electronic switching device named metal-semiconductor field-effect transistor (FET). Thin-film transistors (TFTs) are a special kind of FET made by deposition of semiconductor thin film layers which is acting as an active layer and dielectric layer and metallic contact on a substrate. The journey of TFTs era has started when P.K. Weimer invented a staggered structure of TFT with source and drain contacts on the opposite side of semiconductor thin film layer from the gate at RCA laboratory in 1962 [47]. The semiconductor channel layer of TFTS can be made using various types of semiconductor materials, such as silicon, polycrystalline silicon, organic and compound semiconductor. High field-effect mobility, uniform, and stable TFT technology has attracted great attention for application in next generation flat-panel displays (FPDs).

5.1.1 Amorphous Hydrogenated Silicon (a-Si:H) TFTs

Since 1976, amorphous silicon (a-SI) TFTs have been used in active-matrix flat panel displays, X-ray image sensor and optical scanners as an addressing circuit [48][49][50]. The common feature of amorphous materials is the disorder of atomic structure. For this reason, there is a very high defect in a:Si which limits the performance of the semiconductor devices. To overcome this problem, hydrogenated amorphous silicon (a-Si:H) was described by Lecomber et al. in 1979 and after that has been used in electronic devices because of it has asignificantly low number of defects [51–55]. The a-Si:H TFTs have been widely used in the active-matrix liquid crystal display (AMLCD) industry. However, the stability of a-Si:H TFTs is deteriorated in organic light-emitting diodes (AMOLEDs) displays while employing a-Si:H TFT backplanes on clear plastic substrate. The threshold voltage increases with the time because of the charge trapping in the gate insulator (GI) and defect creation in the a:Si layer [56]. This problem becomes severe for low process temperature TFTs on a clear plastic substrate (<<300 °C). The device performance is limited by low field effect mobility (less than 1 cm^2/V-s) of active channel materials.

Table 5.1: Comparison of different TFT technologies

Items	Poly-Si TFT	a-Si:H TFT	Organic TFT	a-metal oxide TFT
Mobility	~100	<1	1 – 10	>10
Uniformity	Poor	Good	Poor	Good
Scalability	4 G	>10 G	8 G	8 G
Reliability Bias Stress	Very good	Poor	Poor	Good
Reliability light Stress	Very good	Poor	Poor	Good
TFT mask	5 - 9	4 - 5	4 - 5	4 - 5
Cost / Yield	High / low	Low / high	Low / high	Low / high
Process temperature	250 ~ 500 °C	~ 250 °C	<200 °C	RT - 400°C
Deposition method	PECVD	PECVD	Printed, Solution	Sputtering
Band gap	~ 1.5 eV	~ 1.7 eV	2 – 3 eV	~ 3 eV

5.2 Amorphous Oxide TFTs

Amorphous oxide TFTs are widely using as a switching and driving devices for active-matrix flat panel displays (AMFPDs) based on AMLCDs and AMOLEDs, medical imagers, bio-sensors, pressure sensors, low-power communication and energy harvesting [5,57,58]. Different TFTs technologies such as a-Si:H, Poly-Si, metal oxide and organic semiconductors have received great attention for the rapid developments TFTs for next generation displays. Table 5.1 shows the comparisons among different TFT technologies. The electrical properties of poly-Si TFT have better than a-Si:H, such as high carrier mobility (> 100 cm^2/V-s), excellent light and bias stability [59]. Poly-Si is widely used in lightweight, portable, low power and high resolution FPDs because it has some drawback such as the uniformity and scalability due to grain boundaries. On the other hand, a-Si:H TFTs will be difficult to apply in the OLED displays because it has many demerits such as low mobility, electrical bias stress and instability under illumination [60–62]. So higher field-effect mobility, minimum threshold voltage, and high on current are still challenge. Figure 5.1 shows the required mobility of TFT as functions of the number of pixels in the display.

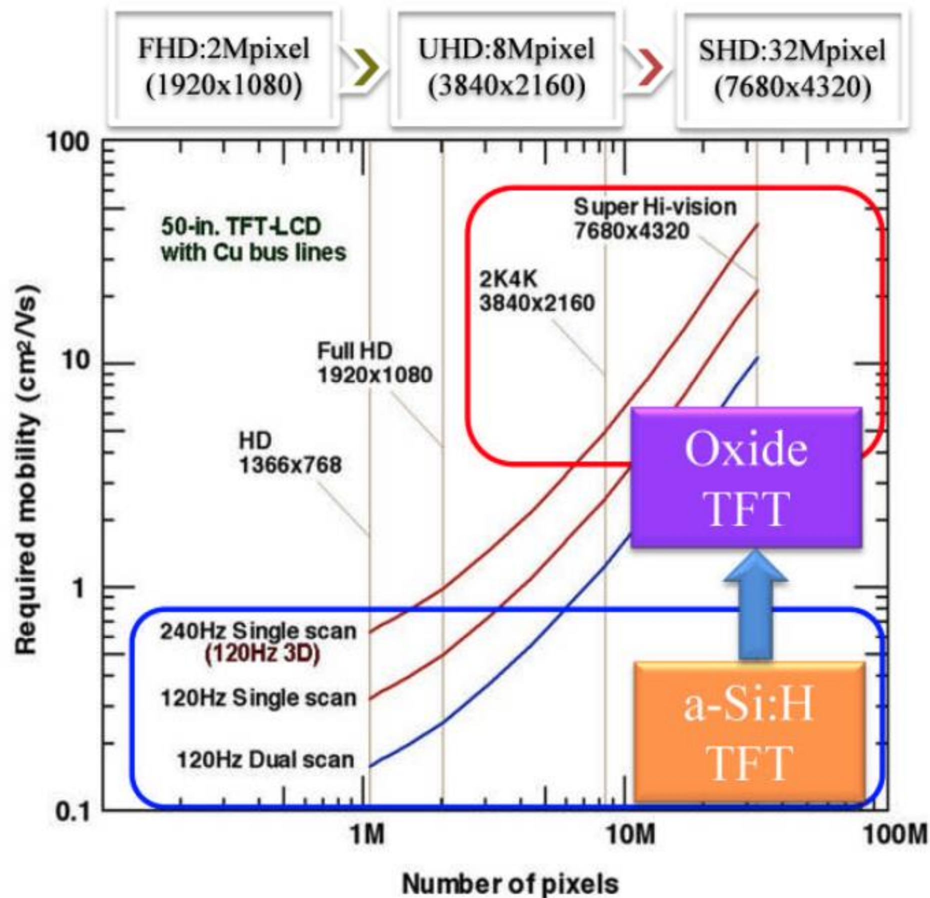

Figure 5.1: Requirement of mobility for higher-definition FPDs

5.3 Current issues on TFT technology

Nowadays Indium–Gallium–Zinc-Oxide (IGZO) thin-film transistors (TFTs) have received considerable research attention as active-matrix backplanes for the next generation display technology [5][63]. Recently, IGZO TFTs are used as a switching device in the flat panel display such as active-matrix organic light-emitting diode (AMOLED) displays, active-matrix liquid crystal displays (AMOLCD) and electrophoretic displays [14][15]. As increasing the resolution (≥ 8 K), display size (≥ 110 inch) and high frame rate (≥ 480 Hz) for the flat panel display; the low-resistance metals are highly required for the source (S) and drain (D) electrodes of IGZO TFTs to reduce resistance-capacitance (RC) delay of display

panel to avoid image distortion and shading [16,64,65]. However, several reports have been revealed that Cu can be a promising material for S/D contact but the diffusion of Cu into IGZO deteriorates the electrical performance because it is acting as acceptor-like trap states of IGZO TFT [66–70]. Recently, a low resistance stacked structure of S/D on IGZO was introduced to enhance the contact properties [71–73]. The Ti and Mo has used widely as an interfacial layer to protect the Cu diffusion into IGZO and to reduce the impact of the Schottky barrier. The work function of Mo and Ti is 4.7 eV and 4.3 eV, respectively which are very closer to IGZO (4.5 eV). In this aspect, Mo-Cu stacked layer is becoming more popular for S/D contact but it is very difficult to pattern the Cu selectively with Cu etchant without damaging active layer which is the main focus in this research.

5.4 Experiments

5.4.1 Fabrication process

An inverted staggered bottom-gate IGZO were prepared on a glass substrate. First, the gate electrode with Al-Nd (85 nm)/ Mo (15 nm) was deposited on a glass substrate by DC magnetron sputtering. Figure 5.2 shows the schematic diagram of DC magnetron sputtering method. Al-Nd alloy is deposited to avoid the electro migration and Mo is used as a barrier layer. The gate electrode was patterned using the photolithography process and wet etching.

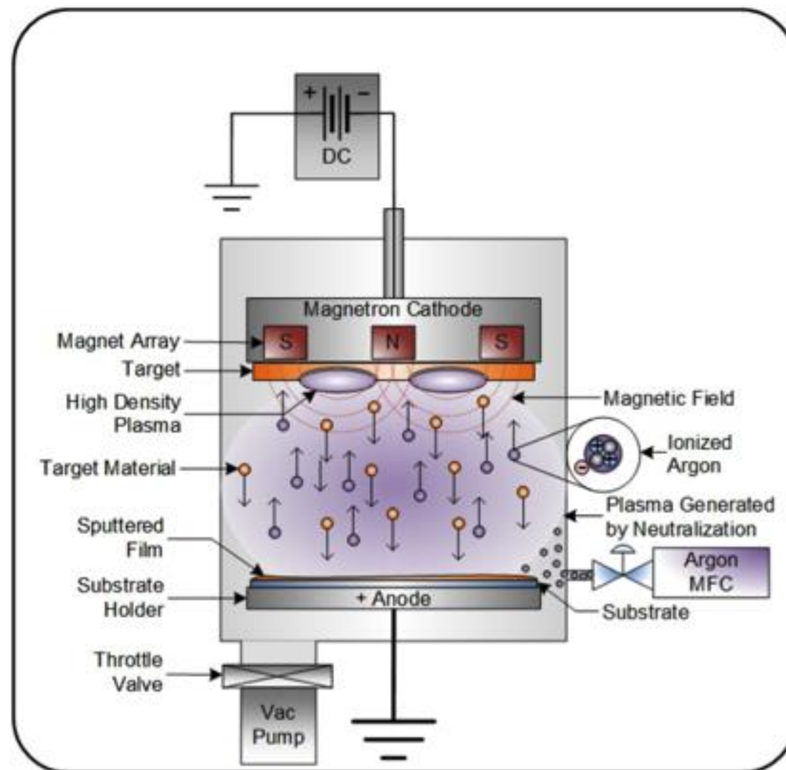

Figure 5.2: Diagram of the DC magnetron sputtering process [74]

Subsequently, a gate insulator (GI) of 150-nm thick SiO_2 was formed using plasma enhanced chemical vapor deposition (PECVD). Then, a 15-nm IGZO thin film as an active layer was deposited by DC magnetron sputtering in the mixture gas of Ar and Ar-O_2 (90%-10%) at 150°C, from the ceramic target atomic ratio In:Ga:Zn = 1:1:1. The deposition chamber pressure was evacuated less than $1x10^5$ Pa and the working pressure was 1 Pa. After that the active layer and GI layer was patterned. The oxygen partial pressure was calculated as [P (O_2) = O_2 / (Ar + O_2)] and fixed at 1%. A 40 nm of 99.999% pure Cu interlayer was deposited on patterned active layer and labelled Sample A [

Figure 5.5 (a)]. Stacked films of 20 nm Mo and 40 nm Cu were deposited using thermal evaporation and patterned again the S/D contact for all samples and labelled Sample B [

Figure 5.5 (b)]. Figure 5.3 shows the process flow of the samples used in this report.

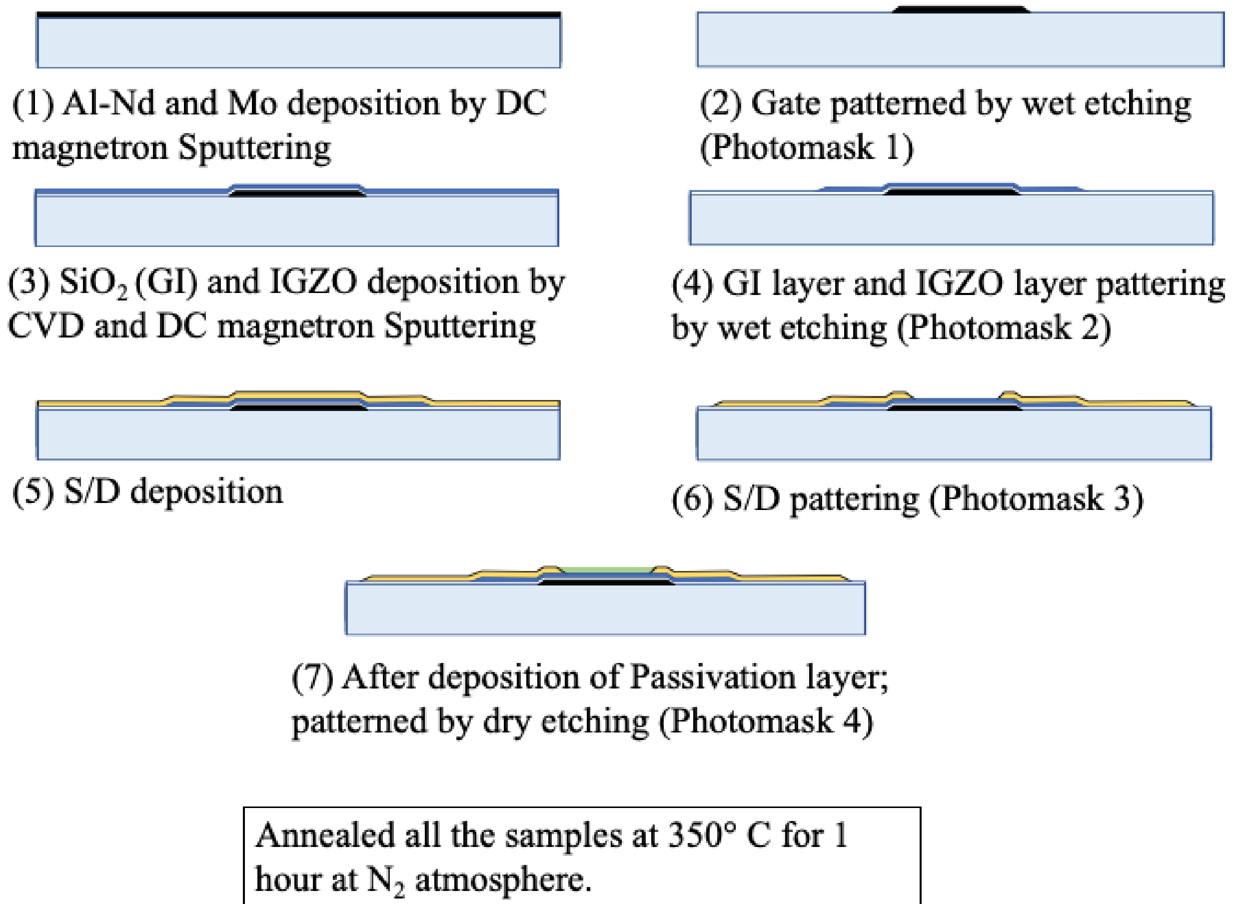

Figure 5.3: Process flow of bottom gate top contact IGZO TFTs.

Thinner Cu layer was deposited to reduce contact resistance, but it is possible to deposit thicker one. The special Cu etchant etch the Cu layer only, which doesn't etch the IGZO active layer. S/D were patterned by photo mask and photolithography process. Active channel width and length were 10 µm and 20 µm, respectively. Finally, 200 nm SiO_2 passivation layer was deposited for both device with working pressure at 110 Pa at 200° C by chemical vapor deposition (CVD) process. Furuta et al. reported that certain amount of H_2 may diffused into IGZO active layer from passivation layer, which can act as a shallow donor in IGZO films [75]. The SiO_2 passivation layer was deposited at the partial pressure of SiH_4 of P[SiH_4] = 1.36 % using N_2, SiH_4 and N_2O gases. This passivation layer was also patterned by photolithography process to make the contact. At the end, all the devices were annealed at

350° C at N_2 environment for 1 hour. Figure 5.4 shows the microscopic image of IGZO TFTs samples with no defects after using Cu etchant.

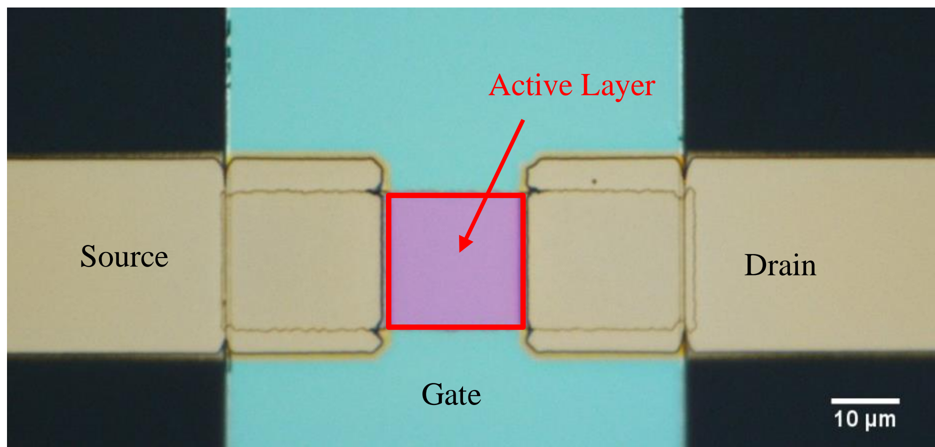

(a)

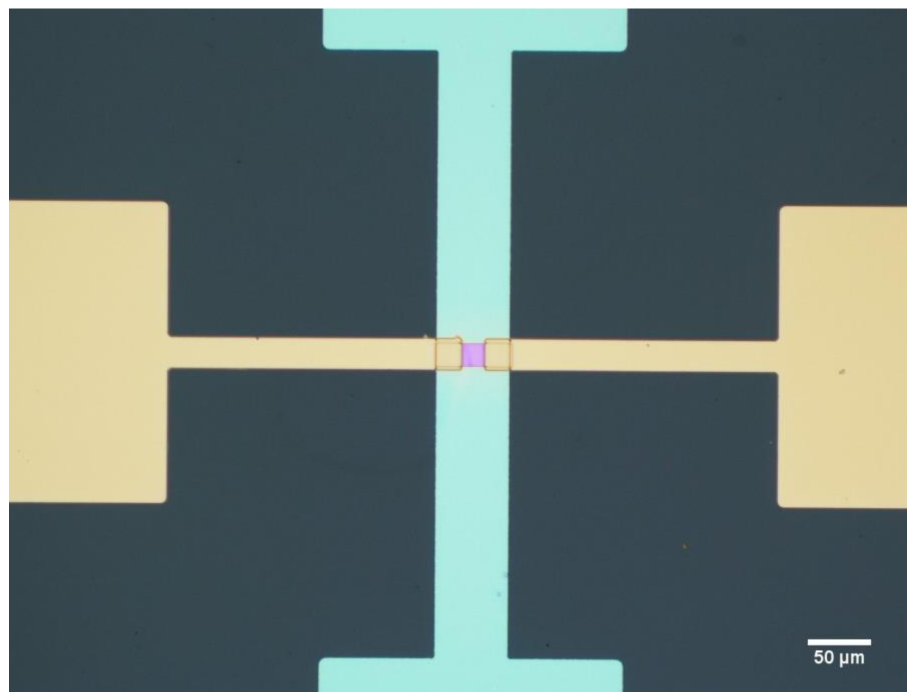

(b)

Figure 5.4: Microscopic image of bottom gate top contact IGZO TFTs after using the special Cu etchant

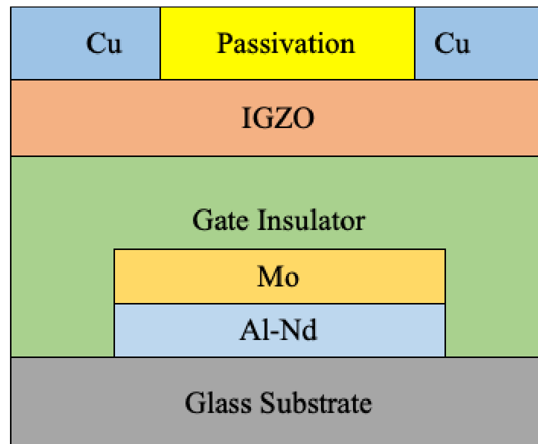

(a)

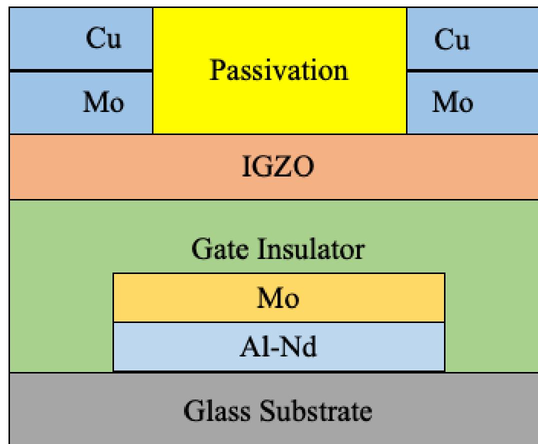

(b)

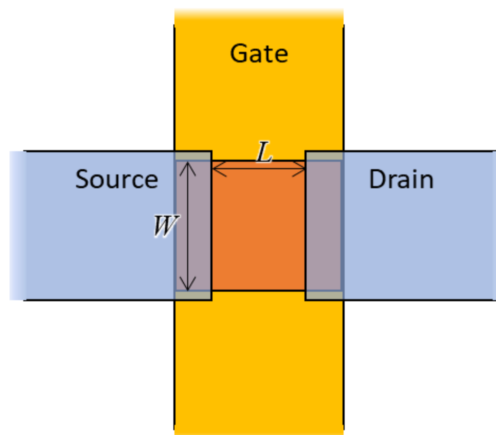

(c)

Figure 5.5: Schematic cross-section of IGZO TFT on a glass substrate with bottom gate top contact structure. (a) sample A, (b) Sample B, and (c) top view of IGZO TFTs.

The active layer defines the channel width, and the separation of S/D electrodes defines the channel length. In this design, the edge of the active layer has a chance to be damaged by the etching. Ferric chloride ($FeCl_3$), Cupric Chloride ($CuCl_2$), Hydrogen peroxide - Sulphuric acid (H_2O_2-H_2SO_4), Chromic - Sulphuric acid (CrO_3-H_2SO_4), ammonium persulphate ($(NH_4)_2SO_4$) and Citric acid are widely used as a Cu etchant but all of them contains strong acid such as HCL and H_2SO_4 [76–78]. All the etchants have high etched rate, high Cu dissolved capacity and very acidic [79]. For this reason, those acidic Cu etchants can damage the IGZO layer and device structure easily and affect the device performance, respectively. Because of this reason, most of the researchers are using shadow mask to deposit S/D to avoid wet Cu etchant [73,80–82]. TFTs characteristics are usually presumed from the transfer characteristics, where the drain to source current (I_d) is plotted against gate to source voltage (V_g) for various drain to source voltage (V_d) and from output characteristics, where I_d is plotted against drain to source voltage (V_d) for various gate to source voltage (V_g). The parameters of the output characteristics, transfer characteristics of sample A and B are as follows; the gate voltage (V_g) was 0 V, 5 V and 10 V and drain voltage was 0.1 V, 5 V and 10 V, respectively. At the value of drain voltage (V_d) at 1 V, threshold voltage (V_{th}) represents the gate voltage (V_g) corresponding to the drain current (I_d) of 1 x 10^{-9} A.

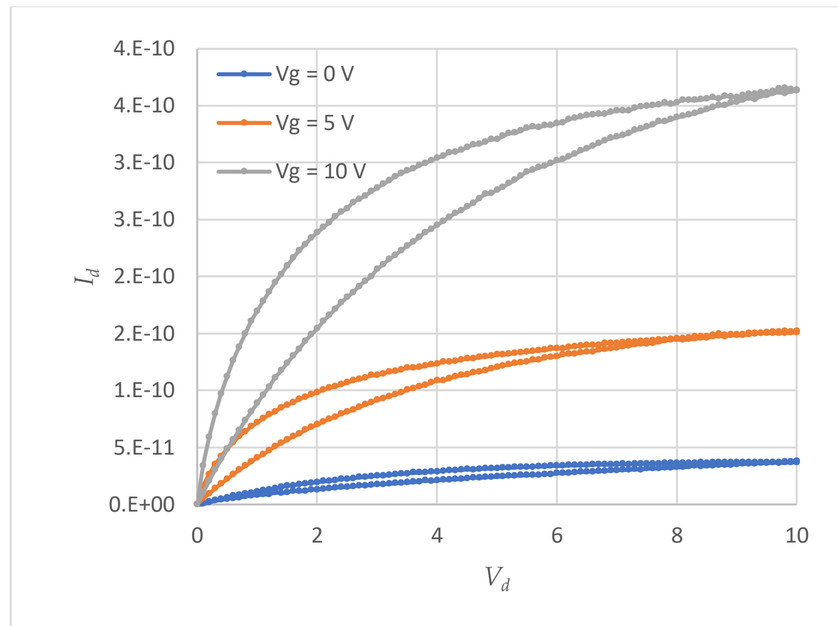

(a)

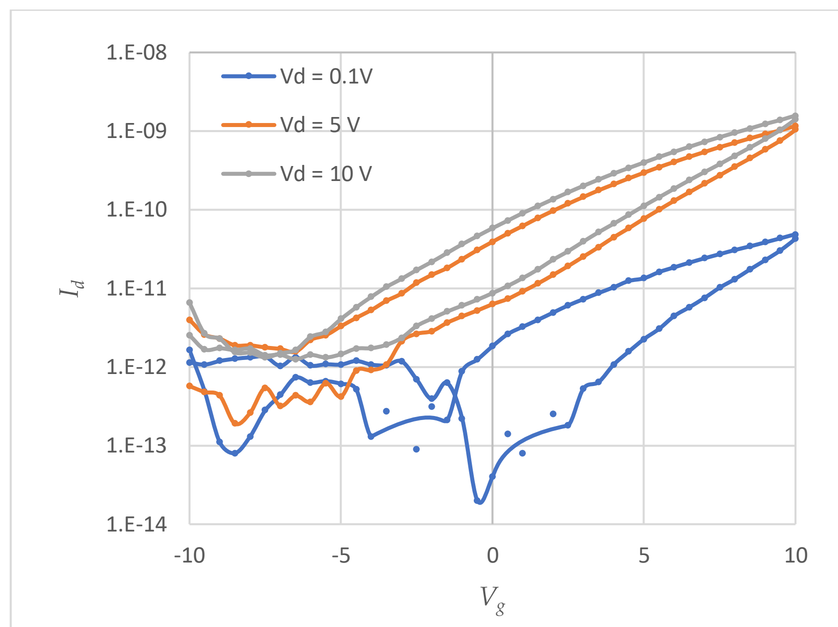

(b)

Figure 5.6: (a) Output and (b) transfer characteristics of sample A without annealing after deposition Cu S/D electrode.

Figure 5.6 and Figure 5.7 represent the output and transfer characteristics of sample A before and after annealing with Cu S/D electrodes. The electrical characteristics of Figure 5.6 are better comparing Figure 5.7, though the mobility is tiny and threshold voltage is quite high. Figure 5.6 is the electrical properties of sample A, which are calculated before annealing the sample with Cu S/D electrode. Therefore, it has less chance of Cu diffusion into IGZO layer. Moreover, the electrical characteristics of sample A after annealing with Cu S/D electrode are becoming worst after post-annealing (Figure 5.7). The reason might be described by the diffusion of Cu into the IGZO layer for post annealing after deposition Cu S/D contact or for depositing Cu onto the channel layer directly.

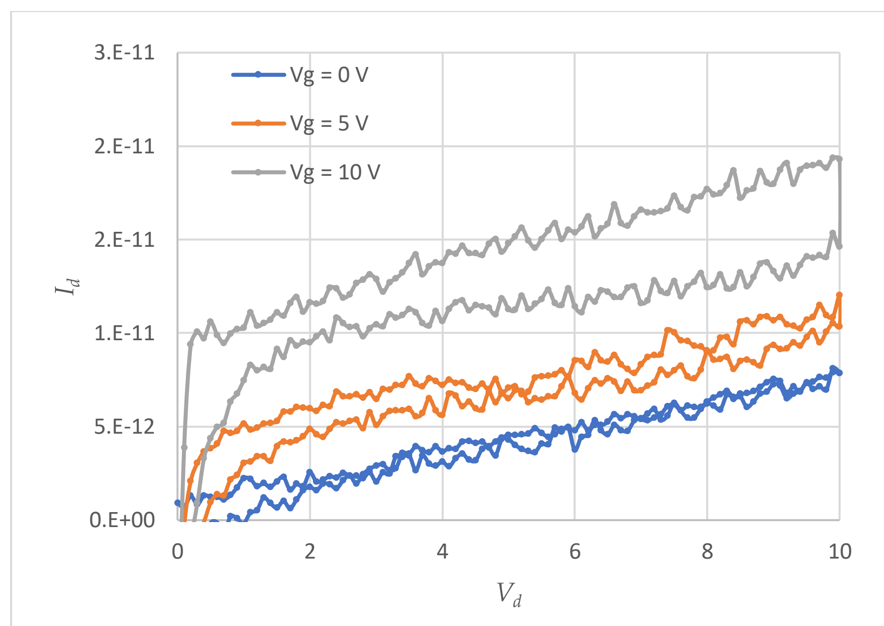

(a)

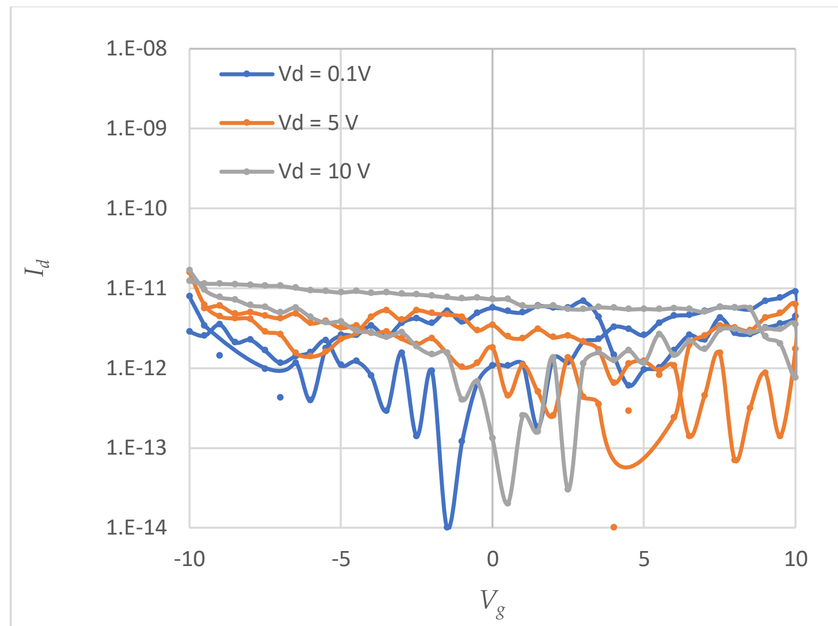

(b)

Figure 5.7: (a) Output and (b) transfer characteristics of sample A with annealing after deposition of CU S/D electrode.

Sample B has a 15-nm thick Mo layer at the S/D contact, which makes ohmic contacts after annealing and prevents the diffusion of Cu into the IGZO layer. Figure 5.8 (a) and (b) show the output and transfer characteristics of sample B after post-annealing with Mo/Cu S/D electrode, respectively. The electrical characteristics of sample shows the good TFT characteristics. The reason might be described that the Mo layer prevents the diffusion of Cu into the IGZO layer after post annealing with deposition of Mo/Cu S/D contact.

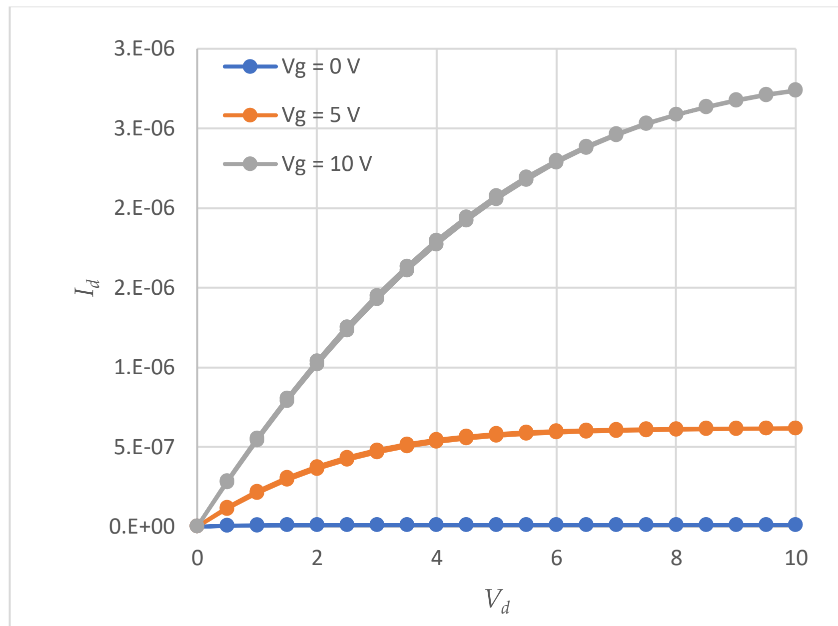

(a)

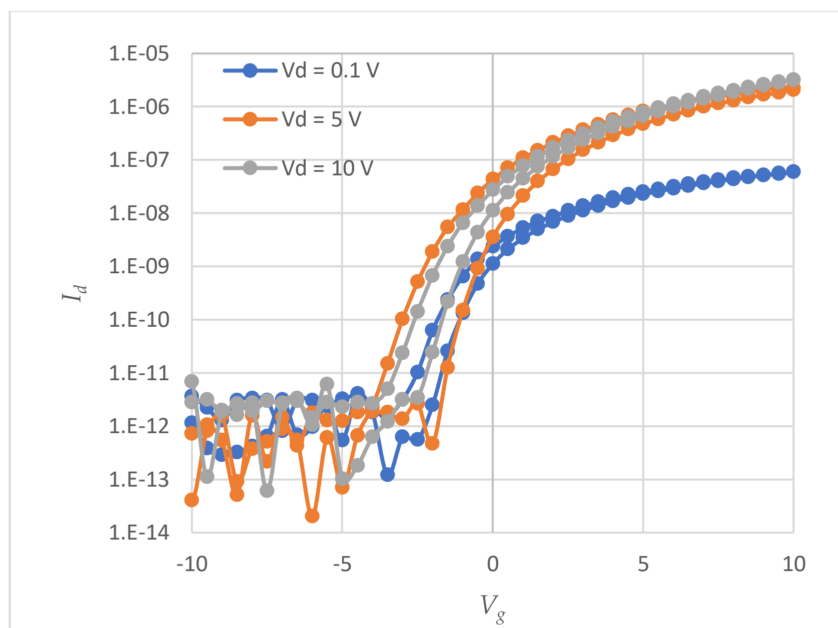

(b)

Figure 5.8: (a) Output and (b) transfer characteristics of sample B after annealing with Mo/Cu S/D electrodes.

The sample B for W/L of 10/20 (µm/µm) achieves improved performance: V_{th} of 1.2 V, μ_{SAT} of 11 cm^2/V-s, and I_{ON} of 3.16x10^{-6} A. This experimental data assure that the non-acidic selective Cu etchant has no effect on IGZO layer. The hysteresis has minimized completely from the output characteristics, but still there is hysteresis at transfer characteristics. The SS value becomes high because the density of acceptor-like trap states of IGZO is also increased. The H_2 atom from passivation layer may diffused into IGZO layer because of annealing, which can enhance the electrical properties. Table 1 exhibits the details analysis between sample A and B after post-annealing.

Table 5.2: Electrical performance of sample A and B after post annealing

S/D	μ_{FE} (cm^2/V-s)	μ_{SAT} (cm^2/V-s)	V_{th} (V)	I_{ON} (A)	*SS* (V/decade)
Cu	9.2×10^{-5}	1.8×10^{-5}	5	1.6×10^{-9}	-
Mo/Cu	12.3	11	1.2	3.2×10^{-6}	0.58

5.5 Conclusion

A back-channel etched Indium–Gallium–Zinc–Oxide (IGZO) thin-film transistors (TFTs) with Cu and Mo/Cu source and drain (S/D) have successfully fabricated using photolithography process. Cu S/D contact using special non-acidic Cu etchant, which can etch Cu properly and avoid the damage to IGZO layer. The electrical properties of IGZO TFTs with Mo/Cu S/D ensure the selectivity of Cu etchant. Post annealing treatment formed an improved the TFT characteristics and Mo interlayer prevented the Cu diffusion into active layer.

Chapter 6

Conclusions and Recommendations

The chapter presents the conclusion on the obtained findings and recommendation on the future work.

6.1 Introduction

In conclusion, the objective of the research are achieved successfully. The method and flow of research are discussed in reflecting to the previous research studies by other researchers. The findings on the research are obtained and described properly. The main findings can be concluded as.

6.1.1 Microstructure analysis of IGZO thin films

6.1.1.1 Analysis from STEM observation

(i) The ADF-STEM observations revealed that nanosized crystals with an average crystal size of 2–5 nm and a lattice distance of approximately 0.24 nm to 0.26 nm were formed in the amorphous matrix of the fabricated IGZO thin films.

(ii) The ADF-STEM observations shows the imperfect crystallinity with local variations in lattice spacing. Because such areas with non-perfect crystallinity overlap with one another along the electron beam direction, it is challenging to directly visualize the local crystallinity. Nevertheless, certain areas showed evident lattice fringes in the amorphous matrix.

(iii)The selected area electron diffraction pattern exhibits certain intensity maxima on the Debye ring. This feature strongly supports the formation of nanocrystals in the IGZO films.

6.1.1.2 Analysis from temperature dependency of thermal conductivity of IGZO thin film using 3ω method

(i) The measured total thermal conductivity of the IGZO thin films increased with an increase in the O_2 / Ar flow ratio. So, thermal conductivity of thin films is proportional to the O_2 flow ratio. It is indicated that the increase in the mean free path of phonons propagating in the films owing to the reduction in the number of oxygen vacancies and the consequent improvement in the nano crystallinity of the films, caused the increase in thermal conductivity.

(ii) The temperature dependent thermal conductivity of IGZO thin films shown a clear demonstration of the significant crystallinity.

(iii) This is because the phonon-phono scattering is increasing with an increase in temperature. This phenomenon is a common feature for all crystalline materials. The mean free path has an inverse proportional relationship with the temperature.

6.2 Application to IGZO TFTs:

(i) The back-channel etched Indium–Gallium–Zinc–Oxide (IGZO) thin-film transistors (TFTs) with copper (Cu) source and drain (S/D) has fabricated successfully which are patterned by a non-acidic selective etchant of Cu.

(i) The experimental data assure that the non-acidic selective Cu etchant has no effect on IGZO layer.

(ii) Post annealed IGZO TFT with Mo/Cu S/D, improved performance: V_{th} of 1.2 V, μ_{SAT} of 11 cm^2/V-s, and I_{ON} of 3.16×10^{-6} A. This result proves that Mo as a barrier layer can prevent the Cu diffusion into IGZO from S/D

6.3 Future Recommendation

(i) Analysis on temperature dependence thermal conductivity, the measurement was conducted at high temperature. The measurement can be done at low temperature.

(ii) At various deposition condition the temperature dependency thermal conductivity measurement can be done to investigate the detail relation between thermal conductivity and microstructure.

(iii)The subthreshold swing of the IGZO TFTS are not good. So there is huge opportunities to improve the device characteristics.

In summary, the research work on IGZO thermal, microstructure and electrical properties are discussed well with the future recommendation.

END

References

[1] H. Yabuta, M. Sano, K. Abe, T. Aiba, T. Den, H. Kumomi, K. Nomura, T. Kamiya, H. Hosono, High-mobility thin-film transistor with amorphous InGaZnO4 channel fabricated by room temperature rf-magnetron sputtering, Appl. Phys. Lett. (2006). https://doi.org/10.1063/1.2353811.

[2] K. Nomura, A. Takagi, T. Kamiya, H. Ohta, M. Hirano, H. Hosono, Amorphous oxide semiconductors for high-performance flexible thin-film transistors, Japanese J. Appl. Physics, Part 1 Regul. Pap. Short Notes Rev. Pap. 45 (2006) 4303–4308. https://doi.org/10.1143/JJAP.45.4303.

[3] M. Kim, J.H. Jeong, H.J. Lee, T.K. Ahn, H.S. Shin, J.S. Park, J.K. Jeong, Y.G. Mo, H.D. Kim, High mobility bottom gate InGaZnO thin film transistors with Si Ox etch stopper, Appl. Phys. Lett. 90 (2007) 1–4. https://doi.org/10.1063/1.2742790.

[4] K. Nomura, H. Ohta, A. Takagi, T. Kamiya, M. Hirano, H. Hosono, Room-temperature fabrication of transparent flexible thin-film transistors using amorphous oxide semiconductors, Nature. 432 (2004) 488–492. https://doi.org/10.1038/nature03090.

[5] Y. Zhu, Y. He, S. Jiang, L. Zhu, C. Chen, Q. Wan, Indium-gallium-zinc-oxide thin-film transistors: Materials, devices, and applications, J. Semicond. 42 (2021). https://doi.org/10.1088/1674-4926/42/3/031101.

[6] J.S. Lee, S. Chang, S.M. Koo, S.Y. Lee, High-performance a-IGZO TFT with

ZrO2gate dielectric fabricated at room temperature, IEEE Electron Device Lett. 31 (2010) 225–227. https://doi.org/10.1109/LED.2009.2038806.

[7] P. Ma, L. Du, Y. Wang, R. Jiang, Q. Xin, Y. Li, dielectric Low voltage operation of IGZO thin film transistors enabled by ultrathin Al 2 O 3 gate dielectric, 023501 (2018) 1–5. https://doi.org/10.1063/1.5003662.

[8] E.M.C. Fortunato, P.M.C. Barquinha, A.C.M.B.G. Pimentel, A.M.F. Gonçalves, A.J.S. Marques, L.M.N. Pereira, R.F.P. Martins, Fully transparent ZnO thin-film transistor produced at room temperature, Adv. Mater. 17 (2005). https://doi.org/10.1002/adma.200400368.

[9] H.-H. Hsieh, C.-C. Wu, Scaling behavior of ZnO transparent thin-film transistors, Appl. Phys. Lett. 89 (2006) 041109. https://doi.org/10.1063/1.2235895.

[10] K. Nomura, H. Ohta, K. Ueda, T. Kamiya, M. Hirano, H. Hosono, Thin-film transistor fabricated in single-crystalline transparent oxide semiconductor, Science (80-.). (2003). https://doi.org/10.1126/science.1083212.

[11] M.G. Kim, M.G. Kanatzidis, A. Facchetti, T.J. Marks, Low-temperature fabrication of high-performance metal oxide thin-film electronics via combustion processing, Nat. Mater. (2011). https://doi.org/10.1038/nmat3011.

[12] A.T.T. Pham, H.K.T. Ta, Y. ren Liu, M. Aminzare, D.P. Wong, T.H. Nguyen, N.K. Pham, T.B.N. Le, T. Seetawan, H. Ju, S. Cho, K.H. Chen, V.C. Tran, T.B. Phan, Effect of annealing temperature on thermoelectric properties of Ga and In dually doped - ZnO thin films, J. Alloys Compd. 747 (2018) 156–165. https://doi.org/10.1016/j.jallcom.2018.02.349.

[13] J.S. Park, H. Kim, I.D. Kim, Overview of electroceramic materials for oxide semiconductor thin film transistors, J. Electroceramics. 32 (2014). https://doi.org/10.1007/s10832-013-9858-0.

[14] J.S. Park, W.J. Maeng, H.S. Kim, J.S. Park, Review of recent developments in amorphous oxide semiconductor thin-film transistor devices, Thin Solid Films. (2012). https://doi.org/10.1016/j.tsf.2011.07.018.

[15] J. Martins, P. Bahubalindruni, A. Rovisco, A. Kiazadeh, R. Martins, E. Fortunato, P. Barquinha, Bias stress and temperature impact on InGaZnO TFTs and circuits, Materials (Basel). 10 (2017). https://doi.org/10.3390/ma10060680.

[16] S.H. Lee, D.J. Oh, A.Y. Hwang, D.S. Han, S. Kim, J.K. Jeong, J.W. Park, Improvement in Device Performance of a-InGaZnO Transistors by Introduction of Ca-Doped Cu Source/Drain Electrode, IEEE Electron Device Lett. (2015). https://doi.org/10.1109/LED.2015.2445348.

[17] G. Chen, HEAT TRANSFER IN MICRO- AND NANOSCALE PHOTONIC DEVICES, Annu. Rev. Heat Transf. 7 (2013). https://doi.org/10.1615/annualrevheattransfer.v7.30.

[18] K.E. Goodson, Y.S. Ju, Heat Conduction in Novel Electronic Films, Annu. Rev. Mater. Sci. (1999). https://doi.org/10.1146/annurev.matsci.29.1.261.

[19] G. Chen, Phonon heat conduction in nanostructures 1, Int. J. Therm. Sci. 39 (2000). https://doi.org/10.1016/S1290-0729(00)00202-7.

[20] D.G. Cahill, H.E. Fischer, T. Klitsner, E.T. Swartz, R.O. Pohl, Thermal conductivity of thin films: Measurements and understanding, J. Vac. Sci. Technol. A Vacuum, Surfaces, Film. 7 (1989). https://doi.org/10.1116/1.576265.

[21] I. Hatta, Thermal diffusivity measurements of thin films and multilayered composites, Int. J. Thermophys. 11 (1990). https://doi.org/10.1007/BF01133562.

[22] T.M. Tritt, Thermal Conductivity: Theory, properties and apllications, 2004.

[23] T. Borca-Tasciuc, W. Liu, J. Liu, K.L. Wang, G. Chen, Anisotropic thermal conductivity of a Si/Ge quantum dot superlattice, Am. Soc. Mech. Eng. Heat Transf.

Div. HTD. 366 (2000).

[24] K.E. Goodson, M.I. Flik, L.T. Su, D.A. Antoniadis, Prediction and measurement of the thermal conductivity of amorphous dielectric layers, J. Heat Transfer. 116 (1994). https://doi.org/10.1115/1.2911402.

[25] F. Völklein, D.P.E. Kessler, Methods for the measurement of thermal conductivity and thermal diffusivity of very thin films and foils, Measurement. 5 (1987). https://doi.org/10.1016/0263-2241(87)90027-3.

[26] Y.C. Tai, C.H. Mastrangelo, R.S. Muller, Thermal conductivity of heavily doped low-pressure chemical vapor deposited polycrystalline silicon films, J. Appl. Phys. 63 (1988). https://doi.org/10.1063/1.339924.

[27] F. Völklein, Thermal conductivity and diffusivity of a thin film SiO2□Si3N4 sandwich system, Thin Solid Films. 188 (1990) 27–33. https://doi.org/10.1016/0040-6090(90)90190-O.

[28] F. Völklein, H. Baltes, A Microstructure for Measurement of Thermal Conductivity of Polysilicon Thin Films, J. Microelectromechanical Syst. 1 (1992). https://doi.org/10.1109/JMEMS.1992.752511.

[29] M. Asheghi, K. Kurabayashi, R. Kasnavi, K.E. Goodson, Thermal conduction in doped single-crystal silicon films, J. Appl. Phys. 91 (2002). https://doi.org/10.1063/1.1458057.

[30] M. Asheghi, Y.K. Leung, S.S. Wong, K.E. Goodson, Phonon-boundary scattering in thin silicon layers, Appl. Phys. Lett. 71 (1997). https://doi.org/10.1063/1.119402.

[31] Y.S. Ju, K.E. Goodson, Phonon scattering in silicon films with thickness of order 100 nm, Appl. Phys. Lett. 74 (1999). https://doi.org/10.1063/1.123994.

[32] G. Dastgeer, M.F. Khan, J. Cha, A.M. Afzal, K.H. Min, B.M. Ko, H. Liu, S. Hong, J. Eom, Black Phosphorus-IGZO van der Waals Diode with Low-Resistivity Metal

Contacts, ACS Appl. Mater. Interfaces. 11 (2019). https://doi.org/10.1021/acsami.8b20231.

[33] K. Ide, K. Nomura, H. Hiramatsu, T. Kamiya, H. Hosono, Structural relaxation in amorphous oxide semiconductor, a-In-Ga-Zn-O, J. Appl. Phys. 111 (2012) 073513. https://doi.org/10.1063/1.3699372.

[34] A. Janotti, C.G. Van De Walle, T. Hiramatsu, M. Nakashima, E. Kikuchi, N. Ishihara, Correlation between crystallinity and oxygen vacancy formation in In – Ga – Zn oxide study by projector augmented wave method Fundamentals of zinc oxide as a semiconductor, (n.d.).

[35] S. Yamazaki, (Invited) Crystalline Oxide Semiconductor Using CAAC-IGZO and its Application, ECS Trans. . 64 (2014) 155–164. https://doi.org/10.1149/06410.0155ecst.

[36] D.A. Chernodoubov, A. V. Inyushkin, Automatic thermal conductivity measurements with 3-omega technique, Rev. Sci. Instrum. 90 (2019) 024904. https://doi.org/10.1063/1.5084103.

[37] Chapter 10. Sputtering and other physical deposition processes, Tribol. Ser. 35 (1999) 153–178. https://doi.org/10.1016/S0167-8922(99)80013-3.

[38] S. Kudo, H. Hagino, S. Tanaka, K. Miyazaki, M. Takashiri, Determining the Thermal Conductivity of Nanocrystalline Bismuth Telluride Thin Films Using the Differential 3ω Method While Accounting for Thermal Contact Resistance, J. Electron. Mater. 44 (2015) 2021–2025. https://doi.org/10.1007/s11664-015-3646-3.

[39] D.G. Cahill, R.O. Pohl, Thermal conductivity of amorphous solids above the plateau, Phys. Rev. B. (1987). https://doi.org/10.1103/PhysRevB.35.4067.

[40] G. Wei, L. Wang, L. Chen, X. Du, C. Xu, X. Zhang, Analysis of Gas Molecule Mean Free Path and Gaseous Thermal Conductivity in Confined Nanoporous Structures, Int. J. Thermophys. 36 (2015). https://doi.org/10.1007/s10765-015-1942-z.

[41] W. Zhu, G. Zheng, S. Cao, H. He, Thermal conductivity of amorphous SiO2 thin film: A molecular dynamics study, Sci. Rep. 8 (2018). https://doi.org/10.1038/s41598-018-28925-6.

[42] Y. Yang, D. Zhong, Y. Liu, D. Meng, L. Wang, N. Wei, G. Ren, R. Yan, Y. Kang, Thermal Transport in Graphene Oxide Films: Theoretical Analysis and Molecular Dynamics Simulation, Nanomaterials. 10 (2020) 285. https://doi.org/10.3390/nano10020285.

[43] B. Cui, L. Zeng, D. Keane, M.J. Bedzyk, D.B. Buchholz, R.P.H. Chang, X. Yu, J. Smith, T.J. Marks, Y. Xia, A.F. Facchetti, J.E. Medvedeva, M. Grayson, Thermal Conductivity Comparison of Indium Gallium Zinc Oxide Thin Films: Dependence on Temperature, Crystallinity, and Porosity, J. Phys. Chem. C. 120 (2016) 7467–7475. https://doi.org/10.1021/acs.jpcc.5b12105.

[44] G. Busch, Early history of the physics and chemistry of semiconductors-from doubts to fact in a hundred years, Eur. J. Phys. 10 (1989). https://doi.org/10.1088/0143-0807/10/4/002.

[45] Host-Guest-Systems Based on Nanoporous Crystals, 2003. https://doi.org/10.1002/3527602674.

[46] T. Peter Brody, The Thin Film Transistor—A Late Flowering Bloom, IEEE Trans. Electron Devices. 31 (1984). https://doi.org/10.1109/T-ED.1984.21762.

[47] P.K. Weimer, The TFT—A New Thin-Film Transistor, Proc. IRE. 50 (1962). https://doi.org/10.1109/JRPROC.1962.288190.

[48] A. Madan, P.G. Le Comber, W.E. Spear, Investigation of the density of localized states in a-Si using the field effect technique, J. Non. Cryst. Solids. 20 (1976). https://doi.org/10.1016/0022-3093(76)90134-4.

[49] D. Gorham, Amorphous and microcrystalline semiconductor devices: Optoelectronic

devices, Microelectronics J. 24 (1993). https://doi.org/10.1016/0026-2692(93)90016-8.

[50] M.J. Powell, The Physics of Amorphous-Silicon Thin-Film Transistors, IEEE Trans. Electron Devices. 36 (1989). https://doi.org/10.1109/16.40933.

[51] R.A. Street, Thin-film transistors, Adv. Mater. (2009). https://doi.org/10.1002/adma.200803211.

[52] C.-S. Yang, L.L. Smith, C.B. Arthur, G.N. Parsons, Stability of low-temperature amorphous silicon thin film transistors formed on glass and transparent plastic substrates, J. Vac. Sci. Technol. B Microelectron. Nanom. Struct. 18 (2000). https://doi.org/10.1116/1.591259.

[53] P.G. Carey, P.M. Smith, S.D. Theiss, P. Wickboldt, Polysilicon thin film transistors fabricated on low temperature plastic substrates, J. Vac. Sci. Technol. A Vacuum, Surfaces, Film. 17 (1999). https://doi.org/10.1116/1.581708.

[54] S.C. Wang, C.F. Yeh, C.K. Huang, Y.T. Dai, Device transfer technology by backside etching (DTBE) for poly-Si thin-film transistors on glass/plastic substrate, Japanese J. Appl. Physics, Part 2 Lett. 42 (2003). https://doi.org/10.1143/jjap.42.l1044.

[55] P.G. Le Comber, W.E. Spear, A. Ghaith, Amorphous-silicon field-effect device and possible application, Electron. Lett. 15 (1979). https://doi.org/10.1049/el:19790126.

[56] M.J. Powell, S.C. Deane, I.D. French, J.R. Hughes, W.I. Milne, A defect-pool model for near-interface states in amorphous silicon thin-film transistors, Philos. Mag. B Phys. Condens. Matter; Stat. Mech. Electron. Opt. Magn. Prop. 63 (1991). https://doi.org/10.1080/01418639108224449.

[57] C.N. Hoth, P. Schilinsky, S. a Choulis, S. Balasubramanian, C.J. Brabec, Applications of Organic and Printed Electronics, 2013.

[58] M. Ito, C. Miyazaki, M. Ishizaki, M. Kon, N. Ikeda, T. Okubo, R. Matsubara, K. Hatta, Y. Ugajin, N. Sekine, Application of amorphous oxide TFT to electrophoretic display,

J. Non. Cryst. Solids. (2008). https://doi.org/10.1016/j.jnoncrysol.2007.10.083.

[59] T. Kamiya, K. Nomura, H. Hosono, Present status of amorphous In-Ga-Zn-O thin-film transistors, Sci. Technol. Adv. Mater. (2010). https://doi.org/10.1088/1468-6996/11/4/044305.

[60] J.H. Jeon, J. Kim, M.K. Ryu, Instability of an amorphous indium gallium zinc oxide TFT under bias and light illumination, J. Korean Phys. Soc. 58 (2011). https://doi.org/10.3938/jkps.58.158.

[61] H. Oh, S.M. Yoon, M.K. Ryu, C.S. Hwang, S. Yang, S.H.K. Park, Photon-accelerated negative bias instability involving subgap states creation in amorphous In-Ga-Zn-O thin film transistor, Appl. Phys. Lett. 97 (2010). https://doi.org/10.1063/1.3510471.

[62] K. Nomura, T. Kamiya, E. Ikenaga, H. Yanagi, K. Kobayashi, H. Hosono, Depth analysis of subgap electronic states in amorphous oxide semiconductor, a-In-Ga-Zn-O, studied by hard x-ray photoelectron spectroscopy, in: J. Appl. Phys., 2011. https://doi.org/10.1063/1.3560769.

[63] R. Khan, M. Ohtaki, S. Hata, K. Miyazaki, R. Hattori, Thermal Conductivity of Nano-Crystallized Indium-Gallium-Zinc Oxide Thin Films Determined by Differential Three-Omega Method, Nanomaterials. 11 (2021). https://doi.org/10.3390/nano11061547.

[64] M. Zhao, M. Xu, H. Ning, R. Xu, J. Zou, H. Tao, L. Wang, J. Peng, Method for Fabricating Amorphous Indium-Zinc-Oxide Thin-Film Transistors With Copper Source and Drain Electrodes, IEEE Electron Device Lett. (2015). https://doi.org/10.1109/LED.2015.2400632.

[65] T. Arai, Oxide-TFT technologies for next-generation AMOLED displays, J. Soc. Inf. Disp. 20 (2012). https://doi.org/10.1889/jsid20.3.156.

[66] W.S. Kim, Y.K. Moon, K.T. Kim, J.H. Lee, B. Du Ahn, J.W. Park, An investigation of

contact resistance between metal electrodes and amorphous gallium-indium-zinc oxide (a-GIZO) thin-film transistors, in: Thin Solid Films, 2010. https://doi.org/10.1016/j.tsf.2010.02.044.

[67] S. Hu, Z. Fang, H. Ning, R. Tao, X. Liu, Y. Zeng, R. Yao, F. Huang, Z. Li, M. Xu, L. Wang, L. Lan, J. Peng, Effect of post treatment for cu-cr source/drain electrodes on a-igzo tfts, Materials (Basel). 9 (2016). https://doi.org/10.3390/ma9080623.

[68] J.R. Yim, S.Y. Jung, H.W. Yeon, J.Y. Kwon, Y.J. Lee, J.H. Lee, Y.C. Joo, Effects of metal electrode on the electrical performance of amorphous In-Ga-Zn-O thin film transistor, Jpn. J. Appl. Phys. (2012). https://doi.org/10.1143/JJAP.51.011401.

[69] C.S. Youn, D.G. Lee, Effects of post heat treatment on the mechanical properties of cold-rolled Ti/Cu clad sheet, Metals (Basel). 10 (2020). https://doi.org/10.3390/met10121672.

[70] I. Fisher, M. Eizenberg, Copper ion diffusion in porous and nonporous SiO2-based dielectrics using bias thermal stress and thermal stress tests, Thin Solid Films. (2008). https://doi.org/10.1016/j.tsf.2007.10.011.

[71] K.-H. Choi, H.-K. Kim, Correlation between Ti source/drain contact and performance of InGaZnO-based thin film transistors, Appl. Phys. Lett. 102 (2013) 052103. https://doi.org/10.1063/1.4790357.

[72] L. Lan, M. Xu, J. Peng, H. Xu, M. Li, D. Luo, J. Zou, H. Tao, L. Wang, R. Yao, Influence of source and drain contacts on the properties of the indium-zinc oxide thin-film transistors based on anodic aluminum oxide gate dielectrics, in: J. Appl. Phys., 2011. https://doi.org/10.1063/1.3660791.

[73] S. Hu, H. Ning, K. Lu, Z. Fang, Y. Li, R. Yao, M. Xu, L. Wang, J. Peng, X. Lu, Mobility enhancement in amorphous in-Ga-Zn-O thin-film transistor by induced metallic in nanoparticles and Cu electrodes, Nanomaterials. 8 (2018).

https://doi.org/10.3390/NANO8040197.

[74] M. Bellardita, A. Di Paola, S. Yurdakal, L. Palmisano, Preparation of catalysts and photocatalysts used for similar processes, in: Heterog. Photocatal. Relationships with Heterog. Catal. Perspect., 2019. https://doi.org/10.1016/B978-0-444-64015-4.00002-X.

[75] T. Toda, D. Wang, J. Jiang, M.P. Hung, M. Furuta, Quantitative analysis of the effect of hydrogen diffusion from silicon oxide etch-stopper layer into amorphous In-Ga-Zn-O on thin-film transistor, IEEE Trans. Electron Devices. 61 (2014). https://doi.org/10.1109/TED.2014.2359739.

[76] O. Çakır, Review of Etchants for Copper and its Alloys in Wet Etching Processes, Key Eng. Mater. 364–366 (2007). https://doi.org/10.4028/www.scientific.net/kem.364-366.460.

[77] K.R. Williams, K. Gupta, M. Wasilik, Etch rates for micromachining processing - Part II, J. Microelectromechanical Syst. 12 (2003). https://doi.org/10.1109/JMEMS.2003.820936.

[78] M. Georgiadou, Richard Alkire, Anisotropic Chemical Etching of Copper Foil, J. Electrochem. Soc. 140 (1993).

[79] H. Noma, T. Nakanishi, Etching process analysis based on etchant flow for high-density build-up substrate, in: Proc. 6th Electron. Packag. Technol. Conf. EPTC 2004, 2004. https://doi.org/10.1109/eptc.2004.1396620.

[80] S. Hu, H. Ning, K. Lu, Z. Fang, R. Tao, R. Yao, J. Zou, M. Xu, L. Wang, J. Peng, Effect of Al2O3 Passivation Layer and Cu Electrodes on High Mobility of Amorphous IZO TFT, IEEE J. Electron Devices Soc. 6 (2018). https://doi.org/10.1109/JEDS.2018.2820003.

[81] S. Hu, K. Lu, H. Ning, Z. Fang, X. Liu, W. Xie, R. Yao, J. Zou, M. Xu, J. Peng, Effect

of ITO Serving as a Barrier Layer for Cu Electrodes on Performance of a-IGZO TFT, IEEE Electron Device Lett. 39 (2018). https://doi.org/10.1109/LED.2018.2800725.

[82] L.Y. Kim, O.K. Kwon, Effects of Stacked Mo-Ti/Cu Source and Drain Electrodes on the Performance of Amorphous In-Ga-Zn-O Thin-Film Transistors, IEEE Electron Device Lett. 39 (2018). https://doi.org/10.1109/LED.2017.2769669.